electronics

MDPI

Article

Wheel Drive Driverless Vehicle Handling and Stability Control Based on Multi-Directional Motion Coupling

Kai Wang, Yi Luo *, Lifang Du, Zhongping Wu and Han Wang

School of Automobile and Transportation, Chengdu Technological University, Chengdu 611730, China; wang_kai@my.swjtu.edu.cn (K.W.); dlfang1@cdtu.edu.cn (L.D.); wzping1@cdtu.edu.cn (Z.W.); whan1@cdtu.edu.cn (H.W.)

* Correspondence: luoyi@cdtu.edu.cn

Abstract: To fully unleash the performance potential of the Wheel Drive Driverless Vehicle (WDDV) and enhance its handling stability across a wide range of extreme operating conditions, this paper proposes a novel approach for designing a multi-directional motion coupling control system. Firstly, an analysis of the unmanned driving modes of the WDDV is conducted, followed by the establishment of a method for defining the control target parameter set for handling stability. Subsequently, a coupled dynamic model that considers the wheel drive counter force is developed. Building this model, a method for estimating the handling stability state is introduced, focusing on improving both handling and stability aspects. Furthermore, by combining the sliding mode control algorithm with the coupled dynamic model, a design methodology for a multi-directional motion coupling control law that adapts to extreme operating conditions is proposed. Finally, through comprehensive simulation experiments and testbed, the effectiveness of the proposed multi-directional motion coupling control system is validated, demonstrating superior handling stability compared to the decoupled control system.

Keywords: control target; handling stability state; motion coupling control; wheel drive driverless vehicle

Citation: Wang, K.; Luo, Y.; Du, L.; Wu, Z.; Wang, H. Wheel Drive Driverless Vehicle Handling and Stability Control Based on Multi-Directional Motion Coupling. *Electronics* **2024**, *13*, 2744. https://doi.org/10.3390/electronics13142744

Academic Editor: Nikolay Hinov

Received: 31 May 2024
Revised: 10 July 2024
Accepted: 10 July 2024
Published: 12 July 2024

1. Introduction

Improving the transport efficiency of vehicles has been an enduring pursuit, necessitating the rational control and optimal utilization of their dynamic performance advantages. The wheel drive vehicle has multiple independent and controllable power units, which can realize the optimal distribution of longitudinal force, lateral force and vertical force of each wheel, so as to improve the handling and stability of the vehicle. The wheel drive system has introduced a novel implementation approach to enhance the dynamic performance of electric vehicles, positioning it as one of the most promising electric vehicle configurations. The wheel drive system adapts to the development needs of electrification and intelligence of automobiles. It has broad application prospects and has been widely studied [1]. Vehicles equipped with wheel drive systems inherit the inherent dynamic performance advantages, thus assuming a pioneering role in bolstering transport efficiency. Consequently, they inevitably confront the imperative of maneuvering stability control under extreme operating conditions. The control of wheel drive vehicles in extreme conditions presents several challenges: the forceful nonlinearity exhibited by the vehicle's dynamic response necessitates a broader scope of state parameters for modeling and analysis; the control system of wheel drive vehicles under extreme conditions must strike a delicate balance between complexity and real-time responsiveness. Intelligent technologies imbue vehicles with an array of perceptual sensing units, advanced planning and decision-making systems, and high-performance computing units [2]. Leveraging such cutting-edge hardware platforms enables the utilization of intelligent algorithms [3–5] to enhance vehicle performance. Therefore, the fusion of wheel drive vehicles and intelligent technologies in the automotive domain holds considerable potential for resolving the issues pertaining to maneuvering

stability control under extreme operating conditions. This integration forms the primary subject of this study: the Wheel Drive Driverless Vehicle (WDDV). The WDDV combines the advantages of wheel drive and driverless vehicle software and hardware, amplifying the complexity of designing its handling and stability control system. To improve the handling and stability of WDDV, addressing the challenges posed by control actuators and controllable degrees of freedom is of paramount importance.

The determination of vehicle handling and stability control objectives usually starts with improving the yaw stability and roll stability of the vehicle. Key state variables for characterizing lateral stability in automobiles include yaw rate and lateral displacement of the center of gravity, which are often directly targeted in the pursuit of lateral stability control [6–14]. Additionally, the distribution of tire forces, which is closely related to tire slip angles, plays a vital role in determining the vehicle's handling stability. Hence, employing the slip angles of the front and rear tires as control targets can also effectively achieve manipulation stability control [15,16]. Restricting the vehicle speed to remain below the maximum permissible speed under given operating conditions serves as an effective means of ensuring driving stability.

Consequently, vehicle roll angle is commonly regarded as a control target for roll stability control [17,18]. In the context of autonomous driving, the maximum achievable speed is also frequently employed as a control target for manipulation stability [19,20]. Furthermore, there is a growing trend to consider multiple parameters as comprehensive control targets [21,22]. Therefore, determining reference values for these control target parameters assumes utmost importance. Common methodologies include the estimation of reference values for control targets under extreme conditions using empirical rules [23,24], as well as techniques such as phase-plane analysis [25,26]. The estimation of reference values for control targets under extreme conditions using empirical parameters or experimental data presents challenges and suffers from issues of accuracy.

Moreover, phase-plane analysis methods [27,28] heavily rely on specific vehicle responses, thereby limiting their applicability across different vehicle models. An ideal approach would involve deriving reference values for control targets under extreme conditions through vehicle dynamics models. However, due to the strong nonlinearity exhibited by vehicle dynamics responses under extreme conditions, modeling becomes challenging, and control systems designed based on complex dynamics models may struggle to meet real-time requirements.

Cooperative control methods for enhancing vehicle handling stability can be categorized into rule-based methods and coupling-based methods. Rule-based methods trigger control strategies based on specific driving conditions and driver input behavior [6,29]. These strategies can be implemented across different electronic control units (ECUs) to reduce computational demands on individual units. However, this approach may introduce oscillations in vehicle states at control activation boundaries, which can undermine control system stability. Moreover, achieving optimal comprehensive vehicle dynamics performance in extreme conditions remains a challenge. Consequently, the increasing computational capabilities of autonomous driving vehicles have prompted a growing emphasis on coupling control methods for multi-actuator systems.

Coupling control strategies, such as four-wheel coupling control [30], four-wheel active steering coupling control [31], coupling control between wheel drive and active steering [32,33], coupling control involving wheel drive, active braking, and active steering [34–42], and coupling control incorporating wheel drive, active braking, active steering, and active suspension [28], have been proposed to improve different aspects of vehicle stability and handling. However, addressing the coupling control problem of WDDV space multi-directional motion requires the development of multi-degree-of-freedom coupling dynamic models specific to vehicle types, enabling direct design of multi-directional control laws. In practical design, model simplification is often necessary to achieve complete solutions for control variables, which may hinder the full representation of nonlinear effects in extreme conditions. Additionally, wheel drive vehicles operating at the limit often utilize

independent wheel torque control to enhance stability, necessitating the consideration of the coupling effect between longitudinal and roll motions in the dynamic modeling of wheel drive vehicles under extreme conditions.

Summarizing the research status, the deficiencies in the existing research are mainly reflected in the following two aspects:

1. Existing research on manipulation stability control targets exhibits certain limitations: the differences between autonomous vehicles and conventional ones are not adequately addressed; a unified and systematic approach to establishing WDDV manipulation stability control targets is lacking.
2. At present, the WDDV handling and stability control method is mainly based on decoupling control, which is difficult to fully consider the influence of the multi-degree-of-freedom coupling relationship of the vehicle, and the influence of the hub drive reaction force is not considered in the design process of the control system.

In summary, the existing research has not fully addressed the control problem of WDDV for stable maneuvering. Achieving stable maneuvering with coupled control for WDDV remains a challenging task that necessitates further investigation. This paper proposes methodologies for establishing precise control objectives and designing coupled control laws tailored specifically to WDDV. The primary contributions of this study are as follows:

1. Beginning with the classification of automated driving levels, incorporating the unmanned driving mode of WDDV, a comprehensive parameter set for control objectives is established. The approach serves as a valuable reference for quantifying the evaluation indicators of maneuvering stability in unmanned driving scenarios.
2. Based on the established WDDV dynamic model suitable for conventional and extreme conditions, the control objectives of handling and stability is derived. These objectives strike a balance between stability and transportation efficiency, making them adaptable to different operating conditions.
3. A sophisticated coupled control law for WDDV's multi-directional motion under extreme operating conditions is formulated. This approach is highly effective in meeting the control requirements for stable maneuvering under extreme operating conditions.

The subsequent organization of this paper is as follows: Section 2 provides a concise introduction to the underlying theory. In Section 2.1, we establish a parameter set for control objectives. Section 2.2 focuses on the development of an 8-degree-of-freedom (8-DOF) coupled dynamic model for WDDV. Section 2.3 provides a methodology for estimating the reference values of control objectives. Section 2.4 presents the design of coupled control laws for multi-directional motion in WDDV. Section 3 presents the simulation analysis and experimental verification. Finally, Section 4 offers conclusions.

2. System Framework and Methodology

2.1. Research on Control Target Parameter of WDDV

To establish the target parameter set for handling and stability control, it is essential to define the evaluation indices for handling and stability. Currently, there exists industry-level, national-level, and international-level standards, such as "GB/T 6323-2014 [43], The Handling and Stability Test Method for Vehicle," "QC/T 480-1999 [44], The Handling and Stability Index Limit and Evaluation Method for Vehicle," and "ISO 3888-2: 2002 Double-shift International Standard Experiment" [45]. However, given the distinct operational characteristics of driverless vehicles compared to traditional vehicles, the conventional handling and stability evaluation methods are insufficient and require adaptation. Consequently, there is a need to update these methods to address the specific requirements of driverless vehicles.

2.1.1. Establish the Evaluation Paradigm of the Handling Stability

The concept of vehicle handling stability encompasses two fundamental aspects: ma handling and stability. Driverless vehicles exhibit diverse handling patterns, including manned driving, human-machine co-driving, and fully autonomous operation. Moreover, the specific handling and stability requirements vary depending on the intended purpose of different types of driverless vehicles. It is crucial to propose evaluation indices for handling and stability that consider both passengers and vehicles, as the conventional evaluation criteria used in traditional driver handling research are no longer applicable to driverless vehicles. When examining stability, the analysis takes into account both vehicle stability and passenger safety, making the proposed stability evaluation criteria still relevant. However, in the driverless context, the stability index for the vehicle as an electromechanical system becomes less restrictive compared to that of traditional vehicles. For instance, even if the vehicle experiences drifting, fishtailing, or a tire slip on one side, it may still maintain operability.

Nevertheless, these extreme phenomena can significantly impact the passengers' sense of security. This study focuses on the WDDV system, which represents an L4-level automated passenger vehicle. To determine the target for handling and stability control in WDDV, it is necessary to consider its general application as a passenger vehicle and establish appropriate evaluation criteria that align with the characteristics of its driverless control mode. The absence of a human driver characterizes the driverless maneuvering pattern of the WDDV. Instead, the WDDV integrates a sensory sensing system, decision-making planning system, and intelligent execution system, which collectively emulate the visual perception, sensory capabilities, cognitive processes, and motor functions of a human driver. This integrated system functions as the virtual driver of the WDDV. For virtual drivers, the key performance criterion lies in their ability to seamlessly manipulate and control the vehicle in accordance with the intended driving objectives, known as motion controllability in autonomous driving. In other words, within the established hardware system's capacity, the WDDV can precisely execute driving actions based on the motion objectives determined by the decision-making planning system, thereby exemplifying its objective motion-tracking ability. Motion tracking in the context of driverless vehicles typically encompasses speed tracking and path tracking, allowing for a clear definition of the handling evaluation indices for the WDDV, specifically in terms of longitudinal speed error and lateral error.

As a passenger vehicle, the evaluation of stability requires consideration of both occupant safety and vehicle endurance. Therefore, the stability evaluation criteria for the WDDV are determined by referring to research findings in traditional vehicle stability assessment. In accordance with the guidelines specified in "QC/T 480-1999, The Handling and Stability Index Limits and Evaluation Methods for Vehicles," the scoring function for assessing the handling and stability of passenger vehicles is as follows:

$$N_z = 1/6\left(N_S + N_J + N_M + N_H + N_Q + N_W\right) \quad (1)$$

where N_S is the comprehensive score of the serpentine driving test. Through the time domain response analysis of yaw rate and steering wheel angle, the scores formed by the two parameters are calculated, respectively, and then the two scores are weighted to obtain the comprehensive score; N_J is the comprehensive score of the steering wheel angle step input test, which is calculated by the time domain response analysis of the yaw rate; N_M is the comprehensive score of the steering wheel angle pulse test, which is calculated by the time domain and frequency domain response analysis of the yaw rate; N_H is the comprehensive score of the steering returnability test, which is obtained by time domain analysis and calculation of yaw rate; N_Q is the comprehensive score of the steering portability test, which is obtained by time domain analysis and calculation of steering wheel steering force; and N_W is the comprehensive score of the steady-state rotation test, which is

obtained by the time domain analysis of roll angle and yaw rate. The comprehensive scores in Equation (1) are all in the percentage system.

With the advancement of vehicle technology, there is a continuous improvement in vehicle handling and stability, resulting in higher load-carrying efficiency. In 2014, the government introduced the latest test methodology for assessing vehicle handling and stability, documented as "GB/T 6323-2014, Test Method of Vehicle Handling and Stability". This updated test method includes a handling and stability assessment centered around the steering wheel. The test primarily focuses on high-speed conditions, where the response speed, sensitivity, and accuracy of steering are tested when the vehicle is running at elevated speeds. Under high-speed driving, small disturbances can also easily make the vehicle dynamic response enter a nonlinear state. The higher the speed, the easier it is for the car to enter the extreme driving condition. The test is closely aligned with the investigation of handling and stability control methods under extreme vehicle conditions in this study. Consequently, in accordance with the prescribed test methodology, the scoring Function (1) has been revised as follows:

$$N_{zc} = 1/7\left(N_S + N_J + N_M + N_H + N_Q + N_W + N_{ZX}\right) \tag{2}$$

where N_{ZX} is the comprehensive score of the handling and stability test in the central area of the steering wheel. From the handling and stability test method of the steering wheel center area, the handling and stability of the vehicle is evaluated by the analysis results of the steering wheel torque and yaw rate. N_{ZX} is also a percentage system.

To facilitate the observation of the relationship between evaluation results of the handling and stability and related evaluation parameters, according to Equation (2) and the influence parameters of each scoring item in the equation, the handling and stability evaluation paradigm of traditional vehicles is as follows:

$$y_t = A_t f_S(\gamma, \delta_s) + B_t f_J(\gamma, \beta) + C_t f_M(\gamma) + D_t f_H(\gamma) + E_t f_Q\left(F_Q\right) + F_t f_W(\varnothing, \gamma) + G_t f_Z\left(\gamma, T_Q\right) \tag{3}$$

where y_t is the comprehensive evaluation result of passenger vehicle handling and stability; γ is yaw rate; β is sideslip angle; δ_s is steering wheel angle; F_Q is the steering force of the steering wheel; V is the speed; and T_Q is the steering wheel torque; $f_S(\gamma, \delta_s)$ is the evaluation function of the serpentine driving test, which describes the calculation method of this result by yaw rate and steering wheel angle in the national standard. $f_J(\gamma, \beta)$ is the evaluation function of the steering wheel angle step input test, which describes the calculation method of the result by yaw rate in the national standard; $f_M(\gamma)$ is the evaluation function of the steering wheel angle pulse test, which describes the calculation method of the result by yaw rate in the national standard; $f_H(\gamma)$ is the evaluation function of the steering returnability test, which describes the calculation method of the result by yaw rate in the national standard; and $f_Q\left(F_Q\right)$ is the evaluation function of the steering portability test, which describes the calculation method of this result by steering wheel steering force in national standards. $f_W(\varnothing, \gamma)$ is the evaluation function of the steady-state rotation test, which describes the calculation method of the result through roll angle and yaw rate in the national standard; $f_Z\left(\gamma, T_Q\right)$ is the evaluation function of the test in the central area of the steering wheel. The calculation method of this result by yaw rate and steering wheel torque in the national standard is described. A_t, B_t, C_t, D_t, E_t, F_t, and G_t are the weight coefficients of each evaluation result.

According to the national standards, δ_s and T_Q in $f_S(\gamma, \delta_s)$ and $f_Z\left(\gamma, T_Q\right)$ are the parameters used to evaluate the handling of real drivers and $f_Q\left(F_Q\right)$ is a function used to evaluate the handling of real drivers. There is no real driver in WDDV; the handling evaluation is realized by longitudinal speed error and lateral error. Therefore, combined with the handling evaluation parameters of WDDV, referring to the evaluation paradigm of the handling and stability Equation (3) for traditional vehicles, the evaluation paradigm of WDDV handling and stability was proposed as follows:

$$y_c = A_c f_{Sc}(\gamma) + B_c f_J(\gamma, \beta) + C_c f_M(\gamma) + D_c f_{CS}(e_s) + E_c f_{LJ}(e_P) + F_c f_H(\gamma) + G_c f_W(\varnothing, \gamma) + H_c f_{Zc}(\gamma) \quad (4)$$

where y_c is the comprehensive evaluation result of the handling and stability; e_s is the longitudinal speed error; e_P is the lateral error; and $f_{CS}(e_s)$ is the evaluation function of vehicle speed tracking test, which describes the method of calculating the result by longitudinal speed error. $f_{LJ}(e_P)$ is the evaluation function of path tracking test, which describes the calculation method of this result by lateral error. $f_J(\gamma, \beta)$, $f_M(\gamma)$, $f_H(\gamma)$, and $f_W(\varnothing, \gamma)$ are the same as the evaluation function of the handling and stability of a traditional vehicle; $f_{Sc}(\gamma)$ is the evaluation function of the serpentine driving test for driverless patterns. The calculation method of the result calculated by the yaw rate is described, which is obtained by referring to the calculation method of $f_S(\gamma, \delta_s)$, without considering the influence of the evaluation parameters for the real driver of the traditional vehicle. $f_{Zc}(\gamma)$ is the evaluation function of the test for the steering wheel center area of the driverless pattern, which describes the calculation method of this result by yaw rate. A_c, B_c, C_c, D_c, E_c, F_c, G_c, and H_c are the weight coefficients of each evaluation result. $f_{CS}(e_s)$ and $f_{LJ}(e_P)$ propose corresponding test conditions and evaluation result calculation methods for the driverless vehicle. To adequately evaluate the handling of WDDV and better describe the controllability of the vehicle in the process of vehicle speed tracking and path tracking, $f_{CS}(e_s)$ and $f_{LJ}(e_P)$ should be able to make a comprehensive evaluation of the rapidity and accuracy of the control response. In addition, in the process of detailed design, the functions $f_{CS}(e_s)$ and $f_{LJ}(e_P)$ should pay attention to the characteristics of virtual drivers and correctly configure the weight coefficients.

In this paper, the target parameter set for the handling and stability control of the WDDV is established by considering the influential factors derived from the evaluation results of handling and stability. Consequently, the investigation does not extensively delve into the evaluation result functions and weight coefficients presented in Equation (4).

2.1.2. Establishment of the Target Parameters Set of Control

The evaluation paradigm for handling and stability, as represented by Equation (4), provides insight into the influence parameters affecting the evaluation results of the WDDV. These parameters encompass lateral error, longitudinal speed error, yaw rate, sideslip angle, and body roll angle. To enhance the handling and stability performance of the WDDV, this research focuses on investigating control methodologies applicable to extreme conditions. Specifically, it explores methods to improve handling and stability by regulating the response of the aforementioned five parameters. Considering the influence parameters derived from the handling and stability evaluation of the WDDV, real-time control processes are affected by factors such as the target path, target speed, target yaw rate, target sideslip angle, target body roll angle, and the corresponding control strategies associated with each target parameter. The path tracking strategy corresponds to the target path, the speed tracking strategy corresponds to the target vehicle speed, the yaw stability control strategy corresponds to the target yaw rate and target sideslip angle, and the roll stability control strategy corresponds to the target body roll angle. Collectively, the target path, target speed, target yaw rate, target sideslip angle, and target body roll angle constitute the control target set for enhancing the handling and stability of the WDDV, as illustrated in Equation (5):

$$CP = [P_d, V_{xd}, \gamma_d, \beta_d, \varnothing_d] \quad (5)$$

where the target path P_d and the target vehicle's speed V_{xd} are handling control targets, and the target yaw rate γ_d, the target sideslip angle β_d, and the target body roll angle $\varnothing_d$ are stability control targets. In the stability control targets, the target yaw rate and the target sideslip angle are the yaw stability control targets, and the target body roll angle is the roll stability control target. In this paper, the principle of cooperative control of handling and stability of WDDV is determined as follows: The primary objective is to enhance handling performance during conventional driving conditions for the WDDV, while also ensuring

stability when the WDDV is driving in extreme conditions. The path tracking strategy, vehicle speed tracking strategy, yaw stability control strategy, and roll stability control strategy constitute the core control strategy set of WDDV.

Therefore, the handling and stability control system of WDDV is a multi-objective and multi-strategy complex control system.

2.2. Dynamics System Modeling

To address the research requirements for handling and stability control of the WDDV, a comprehensive 8-DOF vehicle dynamics model was developed. This model accurately captures the longitudinal, lateral, yaw, and body roll motions of the vehicle, as well as the variations in four-wheel rotation. The stability of wheel drive vehicle is improved by wheel torque independent control under extreme conditions. When the torque of the hub motor is transmitted to the body, the vertical component force generated can change the roll dynamic response of the vehicle. Therefore, the dynamic model used in the design of WDDV handling and stability control system needs to focus on the influence of the hub drive reaction force on the vehicle motion.

2.2.1. Vehicle Dynamics Modeling

The 8-DOF vehicle dynamics model is shown in Figure 1. The body dynamics equation of WDDV was established as follows:

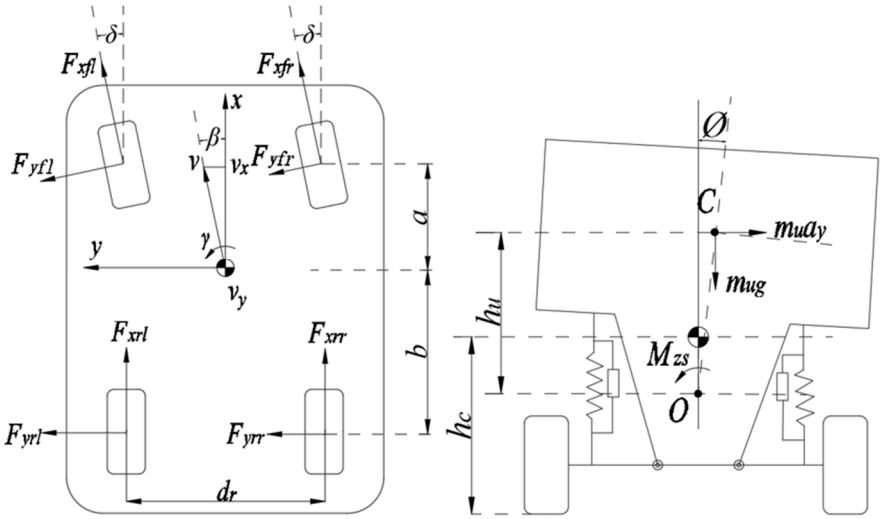

Figure 1. Illustration of 8-DOF vehicle dynamics model.

The longitudinal motion:

$$\Updownarrow\left(\dot{V}_{\mathcal{X}}+V_{\mathcal{Y}}\gamma\right)+m_u h_u\gamma\dot{\phi}=\left(F_{\mathcal{X}fr}+F_{\mathcal{X}fl}\right)cos\delta-\left(F_{\mathcal{Y}fr}+F_{\mathcal{Y}fl}\right)sin\delta+F_{\mathcal{X}rl}+F_{\mathcal{X}rr}-mg(i+f)-\frac{C_D A{V_x}^2}{21.15} \tag{6}$$

The lateral motion:

$$\Updownarrow\left(\dot{V}_{\mathcal{Y}}+V_{\mathcal{X}}\gamma\right)+\left(am_f-bm_r\right)\dot{\gamma}-m_u h_u\ddot{\phi}=\left(F_{\mathcal{Y}fr}+F_{\mathcal{Y}fl}\right)cos\delta+\left(F_{\mathcal{X}fr}+F_{\mathcal{X}fl}\right)sin\delta+F_{\mathcal{Y}rl}+F_{\mathcal{Y}rr} \tag{7}$$

The yaw motion:

$$\begin{aligned}&\left(am_f-bm_r\right)\left(\dot{V}_{\mathcal{Y}}+V_{\mathcal{X}}\gamma\right)+I_z\dot{\gamma}-I_{xz}\ddot{\phi}\\&=a\left(F_{\mathcal{Y}fr}+F_{\mathcal{Y}fl}\right)cos\delta+\tfrac{d_f}{2}\left(F_{\mathcal{Y}fl}-F_{\mathcal{Y}fr}\right)sin\delta-b(F_{\mathcal{Y}rl}+F_{\mathcal{Y}rr})+\tfrac{d_f}{2}\left(F_{\mathcal{X}fr}-F_{\mathcal{X}fl}\right)cos\delta\\&+a\left(F_{\mathcal{X}fr}+F_{\mathcal{X}fl}\right)sin\delta+\tfrac{d_r}{2}(F_{\mathcal{X}rr}-F_{\mathcal{X}rl})\end{aligned} \tag{8}$$

The roll motion:

$$I_x\ddot{\phi}+m_u h_u\left(\dot{V}_{\mathcal{Y}}+V_{\mathcal{X}}\gamma\right)-I_{xz}\dot{\gamma}=\Delta_{df}\left(F_{\mathcal{Y}fr}+F_{\mathcal{Y}fl}\right)cos\delta+\Delta_{dr}(F_{\mathcal{Y}rr}+F_{\mathcal{Y}rl})-D_{\varnothing}\dot{\phi}-(C_{\varnothing}-m_u g h_u)\phi+M_{zs} \tag{9}$$

$$J_w\dot{\omega}_{ij} = T_{dij} - T_{bij} - F_{\mathcal{X}ij}R \tag{10}$$

where ⇳ is the vehicle mass; $V_{\mathcal{X}}$ is the longitudinal speed; $V_{\mathcal{Y}}$ is the lateral speed; m_u is the sprung mass of the vehicle; ϕ is roll angle; $F_{\mathcal{X}ij}$ is the tire's longitudinal force; $F_{\mathcal{Y}ij}$ is the tire lateral force; δ is the average angle of the front wheel; i is the longitudinal slope of the road; f is the tire rolling resistance coefficient; g is the acceleration of gravity; C_D is the air resistance coefficient; A is the windward area of the vehicle; m_f is the springing mass of the front suspension; m_r is the springing mass of the rear suspension; h_{u} is the distance from the center of mass of the sprung mass to the roll axis; I_z is the moment of inertia of the vehicle around the Z axis of the vehicle coordinate system; I_x is the rotational inertia of the vehicle around the X-axis of the vehicle coordinate system; I_{xz} is the inertial product of the whole vehicle in the XZ plane of the vehicle coordinate system; a and b are the distances from the front axle and the rear axle to the center of mass, respectively; d_f and d_r are the front and rear wheel tracks, respectively; M_{zs} is the roll moment generated by wheel drive counter force acting on the body; $D_{\varnothing}$ is the roll-damping coefficient of the vehicle; $C_{\varnothing}$ is the roll stiffness of the vehicle; Δ_{df} is the lateral offset of the front tire caused by unit roll angle; Δ_{dr} is the lateral offset of the rear tire caused by unit roll angle; J_w is the rotational inertia of the wheel; T_{dij} is the wheel driving torque; T_{bij} is the wheel braking torque; and R is the wheel rolling radius (in $\mathcal{X}ij$ or $\mathcal{X}xij$ the footmark i represents f or r, which in turn represents the front wheel or the rear wheel, j represents l or r, which in turn represents the left wheel or the right wheel). The tire force in the model is calculated by the Dugoff nonlinear tire model [46]. The 8-DOF vehicle dynamics model included M_{zs}, which can consider the influence of wheel drive configuration on the roll motion of WDDV. The calculation method of M_{zs} will be studied in detail later.

2.2.2. Analysis of Wheel Drive Counter Force

Previous research by scholars has investigated the influence of wheel drive counterforce on the roll dynamic response of the vehicle body and has established a correlation between the suspension structure and the roll moment M_{zs} [47]. Currently, the WDDV is equipped with a multi-link suspension, but there is limited research available on the wheel drive counterforce specifically related to this suspension type. In most studies, the front and rear suspension systems were projected onto the vehicle's longitudinal plane and the roll moment M_{zs} was calculated through force analysis. Although this calculation method is straightforward, it overlooks the motion coupling relationship between the front and rear suspension systems, as well as the dynamic changes and spatial relationships within the suspension structure. Consequently, significant estimation errors can occur. To address this, this study utilized simulation data fitting to determine the variation pattern of the roll moment M_{zs} induced by the wheel drive counterforce. By considering the generation mechanism of the roll moment M_{zs}, the established dynamic model incorporates the interaction forces between the wheel motor, steering knuckle, suspension rod system, and vehicle body. Furthermore, this dynamic model facilitates the calculation of the roll moment M_{zs} by obtaining the forces at each connection point between the suspension guide rod system and the body. Therefore, a multi-body dynamics model for the WDDV system was developed, and the variation pattern of the roll moment M_{zs} was obtained through simulation.

By analyzing the generation mechanism of roll moment M_{zs}, the main influence parameters of M_{zs} mainly include the driving torque difference between the left wheel and right wheel in wheel motor, steering wheel angle and the height of each quarter suspension. Therefore, the paradigm of M_{zs} is proposed as follows:

$$M_{zs} = f\left(\Delta T_{sf}, \Delta T_{sr}, \delta_{ste}, H_{sfl}, H_{sfr}, H_{srl}, H_{srr}\right) \tag{11}$$

where ΔT_{sf} is the torque difference on the left and right sides of the front axle; ΔT_{sr} is the torque difference between the left and right side of the rear axle; δ_{ste} is the steering wheel angle; H_{sfl} is the suspension height of the first quarter of the left; H_{sfr} is the suspension height of the right front quarter; H_{srl} is the suspension height of the left rear quarter; and H_{srr} is the suspension height of the right rear quarter. The peak torque of the wheel motor

is 1250 Nm, so the value range of ΔT_{sf} and ΔT_{sr} is [–2500, 2500] Nm. According to the range of steering wheel angle of the prototype vehicle, the range of δ_{ste} is determined to be $[-540, 540]^{\circ}$. According to the Wheel jump range of the front suspension and the rear suspension of the vehicle, the value range of H_{sfl}, H_{sfr}, H_{srl}, H_{srr} is determined as $[-70, 50]$ mm. The negative value indicates suspension compression, and the positive value indicates suspension stretching.

Based on the multi-body dynamics model of WDDV, the experimental design was carried out with ΔT_{sf}, ΔT_{sr}, δ_{ste}, H_{sfl}, H_{sfr}, H_{srl}, and H_{srr} in Equation (11) as the influencing factors. Then, the value of M_{zs} under different influencing factors were obtained by simulation and the response surface model of M_{zs} was finally established. Based on the above ideas, firstly, multi-level simulation tests were carried out on the various influencing factors in the Equation (11), and the following conclusions are drawn: the seven influencing factors showed a weak nonlinear relationship with M_{zs}. Therefore, the relationship between each influencing factor and M_{zs} can be described by using fewer levels for each influencing factor. Based on the above analysis, through the value range of each influencing factor, the level of each influencing factor in the test process are determined as follows: ΔT_{sf} and ΔT_{sr} are taken as 8 levels of equal spacing, δ_{ste} is taken as 7 levels of equal spacing, H_{sfl}, H_{sfr}, H_{srl}, and H_{srr} are taken as -70 mm, 0 mm, 50 mm three levels. Finally, the simulation test is carried out according to the comprehensive test method, and the value of M_{zs} under various influencing factors is recorded, and then the response surface model of M_{zs} is obtained by fitting.

Because the dimension of the response surface model is too high to be fully displayed by a figure, the results of M_{zs} response surface under some assumed conditions are shown: (1) Figure 2 shows the response surface model of the body roll moment M_{zs} generated by the wheel motor torque within the allowable range under the uniform linear condition. There was no steering and suspension deformation under this condition, $\delta_{ste} = 0$, $H_{sfl} = 0$ mm, $H_{sfr} = 0$ mm, $H_{srl} = 0$ mm, and $H_{srr} = 0$ mm. The figure shows that the response range of M_{zs} is $[-3390, 2835]$ Nm. (2) Figure 3 shows the response surface model of the body roll moment M_{zs} generated within the allowable range of the wheel motor torque under the right sharp turn condition. In this condition, the steering wheel turned right to the limit, $\delta_{ste} = -540^{\circ}$, the left suspension is compressed, and the right suspension is stretched, $H_{sfl} = 70$ mm, $H_{sfr} = -50$ mm, $H_{srl} = 70$ mm, and $H_{srr} = -50$ mm. From the figure, the response range of M_{zs} is $[-3530, 3050]$ Nm. The above data shows that the response range of M_{zs} is large, and it is necessary to consider the influence of M_{zs} on the roll stability of WDDV in stability control.

In the process of real-time control, the simulation data is imported into the control strategy for direct application. However, large volumes of data occupy a lot of storage space. The mathematical model of M_{zs} is established by regression analysis. In theory, polynomials fit any mathematical model. Therefore, the regression model of M_{zs} is constructed by polynomials. Firstly, a 7-variable quadratic polynomial and 7-variable cubic polynomial were constructed as the regression models of M_{zs}, respectively. Then, based on the data obtained from the above simulation test, the parameters of the regression model were calculated by using the solving function of the multivariate nonlinear regression model in Matlab. Furthermore, the results of the solution were analyzed, and the items in the polynomial that had minimal influence on the results were discarded. Finally, the mathematical model of M_{zs} is determined as follows:

$$\begin{aligned} M_{zs} = (&7{H_{srl}}^2 - 14{H_{srr}}^2 + 3\Delta T_{sf}H_{sfl} + 3\Delta T_{sf}H_{sfr} + 3\Delta T_{sr}H_{sfl} + 3\Delta T_{sr}H_{sfr} + 775\Delta T_{sf} - 12824\Delta T_{sr} - \\ &222\delta_{ste} - 230H_{sfl} + 336H_{sfr} - 1753H_{srl} + 608H_{srr})/10000 \end{aligned} \tag{12}$$

The regression model with Equation (12) as M_{zs} is analyzed, and the root mean square error (RMSE) ≤ 94 N/m. Compared with the vehicle, the value is very small and within the acceptable range. Furthermore, in the process of regression analysis, the absolute value of residuals is less than 250 N/m, and the absolute value of residuals less than 100 N/m

accounts for 86.5% of the total residuals. In summary, the established mathematical model of M_{zs} has high accuracy and meets the research needs.

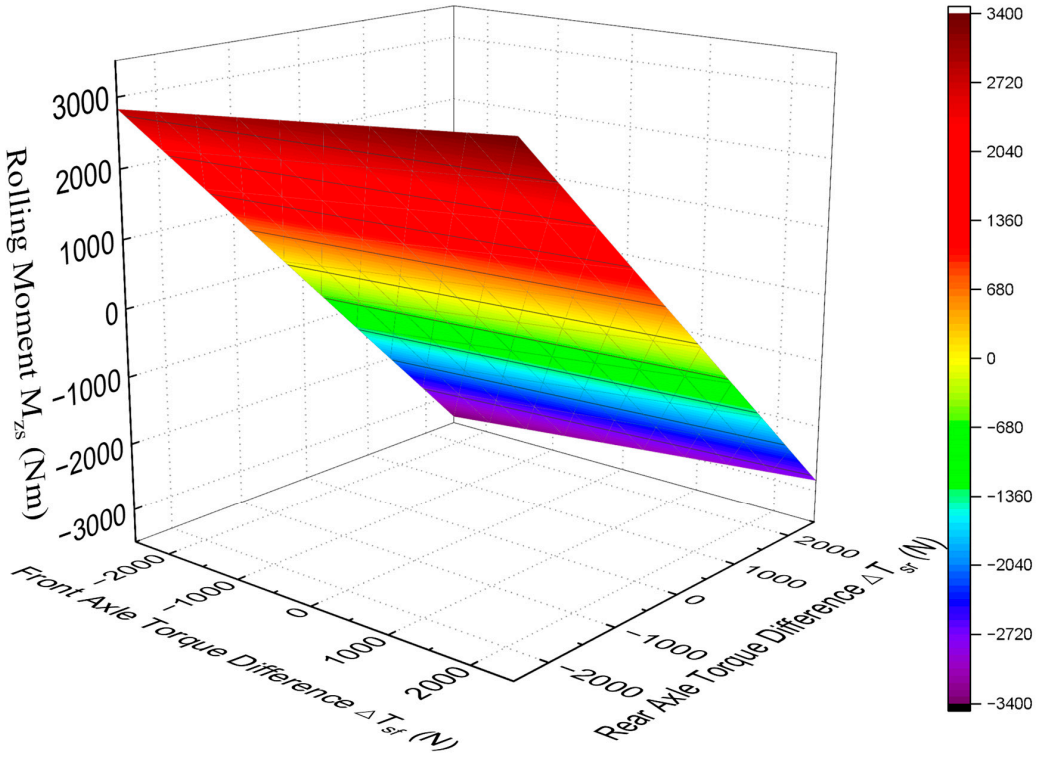

Figure 2. Response surface model of roll moment M_{zs} under uniform linear condition.

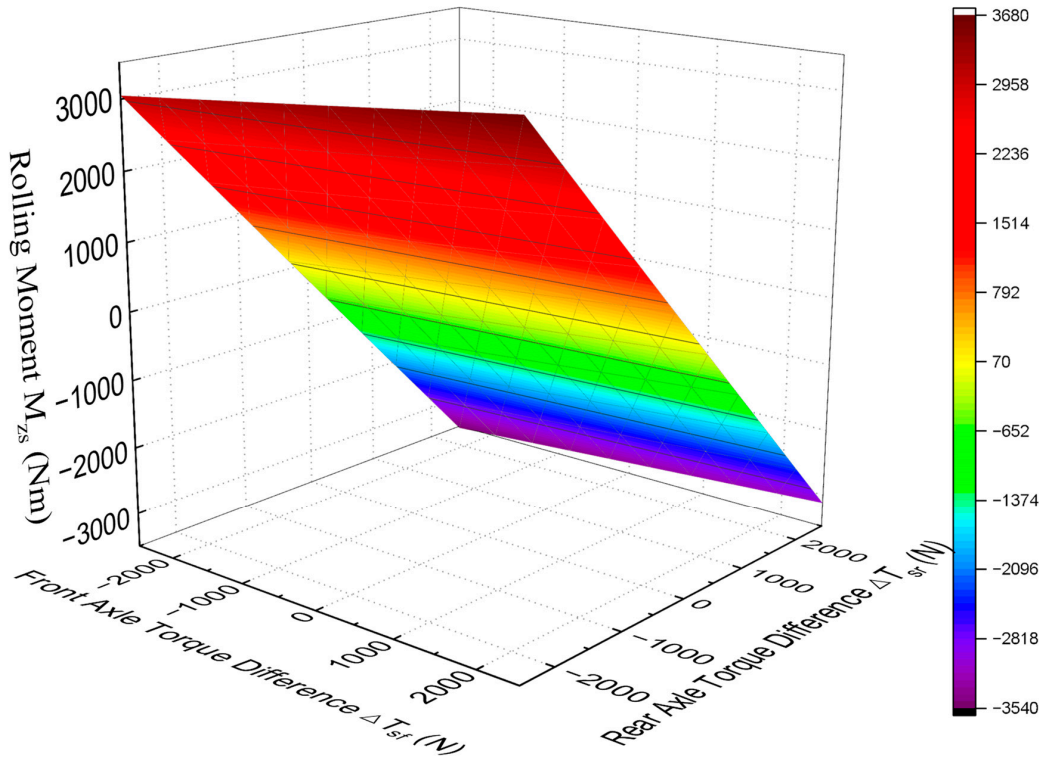

Figure 3. Response surface model of roll moment M_{zs} under a right sharp turn condition.

2.3. Estimation of Reference Values for Control Targets

The handling and stability state of a vehicle encompasses three distinct states: a stable state with weak nonlinearity, an unstable state with strong nonlinearity, and a critical state characterized by a strong dynamic response between these two states. The stable state corresponds to the vehicle operating under normal conditions, while the critical state pertains to extreme conditions, and the unstable state signifies a safety issue with the vehicle. However, this paper focuses solely on the dynamic aspects of the vehicle in the stable state, excluding the investigation of the vehicle's behavior in the unstable state. Under normal conditions, virtual drivers anticipate a specific handling and stability state that aligns with their intended driving behavior. This state ensures the virtual driver's driving intentions are easily accommodated, thereby enabling the driverless vehicle to achieve optimal handling.

Similarly, under extreme conditions, virtual drivers also have an expected handling and stability state. In this state, the driverless vehicle operates at high speeds, pushing the dynamic response of the vehicle to its stability limits. This state represents an ideal condition for enhancing vehicle transportation efficiency. For clarity, we will refer to the aforementioned states as the "expected state of handling" and the "extreme stable state", respectively. This paper aims to investigate the estimation method for determining the expected handling state and stable limit state of WDDV. The estimation results serve as the reference values for controlling the handling and stability of WDDV.

2.3.1. Estimating the Expected State of the Handling

Under conventional conditions, the determination of target speed and target path in WDDV relies on the decision planning module, considering the driver's intention and the driving environment. To ensure stability, the target values for yaw rate, body roll angle, and sideslip angle must be established. The target path and target speed define the desired dynamic response envisioned by the virtual driver. Consequently, the reference value for the stability control target is derived to effectively characterize the expected dynamic response of the virtual driver in conventional conditions. Ultimately, this process yields the anticipated handling state, which is characterized by the expected sideslip angle, yaw rate, and roll angle.

The existing research on the anticipated handling state lacks full applicability to WDDV, primarily due to the following three limitations:

(1) The derived expected state model of vehicle handling is based on a 2-DOF vehicle dynamics model that considers lateral motion and yaw motion. However, it fails to incorporate the expected roll angle, thereby resulting in an incomplete estimation of the anticipated state for WDDV.
(2) The current research commonly employs the average front wheel angle and real-time vehicle speed as inputs to estimate the expected control state. However, this approach inadequately reflects the anticipated state of the virtual driver, which relies on the target vehicle speed and target path as references.
(3) The prevailing studies often derive the expected handling state using a linear vehicle model, neglecting the nonlinear characteristics of the tires. Consequently, the estimation of the desired control state becomes inaccurate as the influence of tire nonlinearity is disregarded.

Considering the limitations observed in previous studies, this research aims to address them by simplifying the established 8-DOF dynamic model and deducing the expected handling state of WDDV based on the requirements for conventional conditions.

Under conventional conditions, the driverless vehicle operates smoothly, adhering to the target path and target speed while accounting for real-time control system demands. The dynamic model is based on the following assumptions:

(1) The vehicle traverses a flat road without any input of vertical road roughness, allowing us to neglect the influence of the tire's vertical force caused by unevenness.

(2) The suspension system is taken into consideration, focusing solely on the roll rotation of the vehicle's sprung mass relative to the unsprung mass. It is assumed that the roll axis of the vehicle remains parallel to the ground, leading to negligible changes in the wheel steering angles ($\Delta_{df} \approx 0$, $\Delta_{dr} \approx 0$). This assumption disregards the effects of suspension deformation on wheel steering angles and the vertical displacement of the vehicle's centroid caused by the relative vertical motion between the partially sprung mass and unsprung mass.

(3) The vehicle's speed changes gradually without rapid acceleration or deceleration, maintaining a constant value. Consequently, the dynamic differential equation governing longitudinal motion can be omitted.

(4) The consideration of aerodynamics is omitted from the model.

(5) In the context of conventional conditions, emergency sharp turns are not encountered, resulting in a small value for the steering angle (δ). Consequently, approximations can be made such that $\sin\delta \approx \delta$ and $\cos\delta \approx 1$.

(6) Under conventional conditions, WDDV maintains stability, eliminating the need to enhance stability through torque vector control of the wheel motor. Hence, the counter force exerted by the wheel drive has minimal impact on the vehicle body's roll motion, leading to $M_{zs} \approx 0$.

Consequently, WDDV can be simplified into a monorail model, considering both the sprung mass and unsprung mass. This simplified vehicle dynamics model accounts for longitudinal, lateral, yaw, and roll motion, supported by front and rear elastic tires interacting with the ground. Finally, by combining Equations (7)–(9) with the simplified Dugoff tire model [48], which is suitable for conventional conditions, the simplified vehicle dynamics equations for WDDV, describing longitudinal motion, lateral motion, yaw motion, and roll motion can be established as follows:

The lateral motion:

$$\Updownarrow\left(\dot{V}_{\mathcal{Y}} + V_{xd}\gamma\right) + \left(am_f - bm_r\right)\dot{\gamma} - m_u h_u \ddot{\phi} = C_{\mathcal{Y}f} f\left(\sigma_f\right)\left(\beta + \frac{a\gamma}{V_{xd}} - \delta_d\right) + C_{\mathcal{Y}r} f(\sigma_r)\left(\beta - \frac{b\gamma}{V_{xd}}\right) \tag{13}$$

The yaw motion:

$$\left(am_f - bm_r\right)\left(\dot{V}_{\mathcal{Y}} + V_{xd}\gamma\right) + I_z\dot{\gamma} - I_{xz}\ddot{\phi} = aC_{\mathcal{Y}f} f\left(\sigma_f\right)\left(\beta + \frac{a\gamma}{V_{xd}} - \delta_d\right) - bC_{\mathcal{Y}r} f(\sigma_r)\left(\beta - \frac{b\gamma}{V_{xd}}\right) \tag{14}$$

The roll motion:

$$I_x\ddot{\phi} + m_u h_u\left(\dot{V}_{\mathcal{Y}} + V_{xd}\gamma\right) - I_{xz}\dot{\gamma} = -D_{\varnothing}\dot{\phi} - (C_{\varnothing} - m_u g h_u)\phi \tag{15}$$

where δ_d is the average rotation angle of the expected front wheel to achieve the target path tracking calculation. $C_{\mathcal{Y}f}$ is the equivalent slip angle stiffness of the front axle tire; $C_{\mathcal{Y}r}$ is the equivalent slip angle stiffness of the rear axle tire; and $f\left(\sigma_f\right)$ is the coefficient equation in the Dugoff tire model [48]. The simplified vehicle dynamics model takes the target speed V_{xd} and the δ_d calculated according to the target path as input, which is more conducive to describing the expected vehicle dynamics response of the virtual driver and has the characteristics of the driverless vehicle.

In conventional conditions, the curvature of the target speed and target path changes slowly. When the corresponding target speed and target path are reached and stabilized during the driving of the WDDV, $\dot{V}_{\mathcal{Y}} \approx 0$, $\dot{\gamma} \approx 0$, $\dot{\phi} \approx 0$, $\ddot{\phi} \approx 0$. Further, combined with the simplified WDDV vehicle dynamics Equations (13)–(15), the expected state of the handling of WDDV is obtained as follows:

$$\gamma_{s\mu} = \frac{V_{xd}}{L\left(1 + K_\mu V_{xd}^2\right)}\,\delta_d \tag{16}$$

$$\beta_{s\mu} = \frac{b + \frac{V_{xd}^2\left(am + bm_r - am_f\right)}{C_{\mathcal{Y}f} f(\sigma_r) L}}{L\left(1 + K_\mu V_{xd}^2\right)}\,\delta_d \tag{17}$$

$$\phi_{s\mu} = \frac{V_{xd}^2 m_u h_u}{L\left(1 + K_\mu V_{xd}^2\right)\left(m_u g h_u - C_\varnothing\right)} \delta_d \tag{18}$$

where $\gamma_{s\mu}$ is the yaw rate expected by the virtual driver; $\beta_{s\mu}$ is the sideslip angle expected by the virtual driver; $\phi_{s\mu}$ is the expected roll angle of the virtual driver; and K_μ is the stability factor derived from the estimation of the expected state of the handling of WDDV. Compared with the stability factor K [49], K_μ considers the effects of unsprung mass, road adhesion characteristics, and tire nonlinearity on vehicle stability. The expression of K_μ is similar to K, as follows:

$$K_\mu = \frac{1}{L^2}\left[m\left(\frac{a}{C_{\gamma r} f(\sigma_r)} - \frac{b}{C_{\gamma f} f\left(\sigma_f\right)}\right) + \left(b m_r - a m_f\right)\left(\frac{1}{C_{\gamma r} f(\sigma_r)} + \frac{1}{C_{\gamma f} f\left(\sigma_f\right)}\right)\right] \tag{19}$$

where K is expressed as: $K = 1/L^2\left[m\left(a/C_{\gamma r} f(\sigma_r) - \mathrm{b}/C_{\gamma f} f\left(\sigma_f\right)\right)\right]$. The stability factor of the vehicle is affected by many factors, and the expression of K and K_μ is not accurate. From the expression form and derivation process of K and K_μ, the difference between K_μ and K is that K_μ replaces the original tire linear stiffness with nonlinear stiffness. Because K_μ is derived from the simplified WDDV dynamics model considering the sprung mass and unsprung mass, respectively, and K is derived from the 2-DOF vehicle dynamics model with the sprung mass and unsprung mass as a whole. Therefore, the expression K_μ contains the parameter term composed of unsprung mass. In essence, K and K_μ are both stability factors. Their connotations and different values have the same influence on the stability of the vehicle. Compared with K, K_μ can consider the influence of the unsprung mass and tire nonlinearity on the stability factor. In theory, the stability factor of the vehicle can be calculated more accurately by the expression of K_μ.

The expected state of the handling of WDDV is composed of $\gamma_{s\mu}$, $\beta_{s\mu}$ and $\phi_{s\mu}$. Considering the influence of road adhesion characteristics and load changes on tire cornering stiffness through the function $f(\sigma_i)$, the influence of tire nonlinearity on vehicle handling under different driving conditions can be considered.

2.3.2. Estimating the Stabilization of Extreme State

Under extreme conditions, the WDDV decision-planning module determines the target path based on driving intention and environmental factors, resulting in the remaining control targets reaching their limits. Estimation of the limit values for target yaw rate, target sideslip angle, target body roll angle, and target speed become crucial. The root cause of vehicle instability lies in the insufficiency of tire-generated forces to sustain stable driving. To ensure the stable operation of WDDV under extreme conditions, it is imperative to describe the limit dynamic response state that adheres to the maximum adhesion force provided by the tire and determine the stability control target.

By considering the maximum tire adhesion as a constraint, the calculation model for determining the limit value of the target yaw rate and target sideslip angle can be derived as follows [28]:

$$|\gamma_{max}| = \frac{\sqrt{(\mu g)^2 - \left(a_x + g(i+f) + \frac{C_D A V_x^2}{21.15m}\right)^2}}{|V_\mathcal{X}|} \tag{20}$$

$$\beta_{max} = \gamma_{max}\left(\frac{b}{V_\mathcal{X}} - \frac{V_\mathcal{X}\left(am + bm_r - am_f\right)}{C_{\gamma f} f(\sigma_r) L}\right) \tag{21}$$

where γ_{max} is the limit value of the target yaw rate; β_{max} is the limit value of the target sideslip angle; and τ_γ is the safety factor, and the value is greater than 0 and less than 1. Considering many practical factors that are not taken into account in the modeling process, the appropriate safety margin is retained. a_x is the longitudinal acceleration; L is the wheelbase.

Under extreme conditions, WDDV frequently enhances lateral stability by employing independent control of torque applied to the left and right wheels. During such instances, the wheel drive counter force becomes significant, necessitating careful consideration of the generated body roll torque. The vehicle's roll instability during driving is primarily observed in the form of rollover or sideslip. Consequently, the dynamic model equations for WDDV's rollover and sideslip are established as follows:

$$m_u h_c |a_y| + \left(m_f + m_r\right) R |a_y| = m_u g \left(\frac{d_f + d_r}{4} - |\varnothing| h_u\right) + m g h_c \alpha_{ro} + \frac{\left(m_f + m_r\right) g \left(d_f + d_r\right)}{4} + M_{zs} \tag{22}$$

$$m_u h_c |a_{ymax}| + \left(m_f + m_r\right) R |a_{ymax}| = m_u g \left(\frac{d_f + d_r}{4} - |\varnothing| h_u\right) + m g h_c \alpha_{ro} - \left(F_{zfx} + F_{zrx}\right) \frac{d_f + d_r}{2} + M_{zs} \tag{23}$$

where h_c is the height of the vehicle's center of gravity; α_{ro} is the lateral slope of the road; a_y is the lateral acceleration; a_{ymax} is the maximum lateral acceleration that the vehicle can achieve in stable driving; F_{zfx} is the vertical force of the front wheel unilateral tire; and F_{zrx} is the vertical force of the rear wheel unilateral tire of the vehicle. When a_{ymax} points to the left side of the driving direction of the vehicle, $F_{zfx} = F_{zfl}$, $F_{zrx} = F_{zrl}$. When a_{ymax} points to the right side of the driving direction of the vehicle, $F_{zfx} = F_{zfr}$, $F_{zrx} = F_{zrr}$. The roll model considers the influence of wheel drive configuration on roll stability through M_{zs}.

The maximum roll angle under the critical state of vehicle rollover is as follows:

$$|\varnothing_{max1}| = \frac{m g \left(\frac{d_f + d_r}{4} + h_c \alpha_{ro}\right) - |a_y| \left[R\left(m_f + m_r\right) + h_c m_u\right] + M_{zs}}{m_u g h_u} \tag{24}$$

With the maximum adhesion of the tire as the constraint, combined with Equation (23), the maximum roll angle of the vehicle in the critical state of sideslip is as follows:

$$|\varnothing_{max2}| = \frac{m_u g \frac{d_f + d_r}{4} + m g h_c \alpha - \left(F_{zfx} + F_{zrx}\right) \frac{d_f + d_r}{2} - \sqrt{(\mu g)^2 - \left(a_x + g(i+f) + \frac{C_D A V_x}{21.15m}\right)^2} \left[R\left(m_f + m_r\right) + h_c m_u\right] + M_{zs}}{m_u g h_u} \tag{25}$$

The maximum target roll angle of WDDV is as follows:

$$|\varnothing_{max}| = min(|\varnothing_{max1}|, |\varnothing_{max2}|) \tau_{\varnothing} \tag{26}$$

where $\tau_{\varnothing}$ is the maximum roll angle safety factor of the vehicle, which is greater than 0 and less than 1. To account for numerous practical factors that are not considered during the modeling process, an appropriate safety margin is maintained.

From the above analysis, the γ_{max}, β_{max} and $\varnothing_{max}$ are the important part of the extreme state of the vehicle's stable driving. In the estimation process of γ_{max} and β_{max}, the longitudinal acceleration a_x, lateral acceleration a_y and roll angle $\varnothing$ are obtained by the sensor. The road longitudinal slope i and the road lateral slope α_{ro} are obtained by high-precision map. Based on the camera and radar, the road adhesion coefficient μ is estimated. The longitudinal speed $V_{\mathcal{X}}$ is obtained by the sensor (integrated navigation system), or by estimation. The extreme state estimation method of yaw stability plays the intelligent advantage of WDDV.

Owing to the dynamic nature of speed limits under random conditions, their real-time identification and subsequent tracking and control pose significant challenges. Leveraging the intelligent capabilities inherent in WDDV, a predictive approach for estimating the limit speed is proposed. For a detailed exposition of this method, the author refers to their prior research findings [28].

2.4. Design of Multi-Directional Motion Coupling Control Law

2.4.1. Analysis of Coupling Control Principle

The dynamic coupling characteristics of the vehicle system manifest through the interplay among the motion relationship, tire forces, and dynamic load distribution. Equations (6)–(9) elucidate the following aspects:

(1) The established 8-DOF vehicle dynamics model equation for WDDV encompasses longitudinal speed $V_{\mathcal{X}}$, lateral speed $V_{\mathcal{Y}}$, yaw rate γ, and roll angle ϕ. Alterations in motion parameters in any direction induce corresponding changes in the motion response of the other three directions, highlighting the coupling characteristics inherent in the vehicle's motion relationship.

(2) The equations governing motion in each direction incorporate the longitudinal force $F_{\mathcal{X}ij}$ and lateral force $F_{\mathcal{Y}ij}$ exerted by the tires. The roll motion equation accounts for the body roll torque arising from the wheel drive counter force, which is engendered by the longitudinal force exerted by the wheel motor through the tire and onto the ground. The Dugoff tire model is employed to calculate the longitudinal and lateral forces of the tire, with the model relying on the tire's vertical force as input. By incorporating the Dugoff tire model, the vehicle dynamics model effectively captures the coupling characteristics of tire forces.

(3) During driving, braking, steering, and other operational scenarios, the redistribution of the vertical load on the four wheels occurs due to changes in the centroid position and the effects of inertia. The coupling relationship of tire forces leads to alterations in the longitudinal and lateral forces exerted by the tires, subsequently affecting the overall vehicle response. By employing the Dugoff tire model, the vehicle dynamics model takes into account the dynamic variations in wheel vertical load and its impact on the dynamic response of WDDV.

The 8-DOF vehicle dynamics model for WDDV has been devised to comprehensively address the dynamic coupling characteristics inherent in the system. Building upon this dynamic model, an all-direction motion control law is formulated for WDDV, serving as the foundation for achieving multi-directional motion coupling control within the WDDV space. Moreover, the sliding mode control algorithm, renowned for its swift response, robustness against parameter variations and disturbances, independence from online system identification, and straightforward physical implementation, has garnered significant attention from industry scholars for actively regulating vehicle dynamics performance [50]. Therefore, this study adopts the sliding mode algorithm to design the Multi-directional Motion Coupling Control System (MMCCS) for WDDV.

The MMCCS of WDDV is shown in the dotted box in Figure 4. The input parameters of MMCCS are road adhesion coefficient μ, road longitudinal slope i, yaw angle ψ_R, and other parameters of the WDDV perception fusion module and decision planning module. Other commonly used input parameters for vehicle dynamic performance control include tire force ($F_{\mathcal{Y}ij}$, $F_{\mathcal{X}ij}$, F_{zij}), longitudinal speed $V_{\mathcal{X}}$, lateral speed $V_{\mathcal{Y}}$, yaw rate γ, sideslip angle β, body roll angle ϕ, etc. These parameters include the control target parameters that have been identified in the previous study, including the target path point set (X_n, Y_n), the target vehicle speed $V_{\mathcal{X}d}$, the expected state of the handling: $\gamma_{s\mu}$, $\beta_{s\mu}$, $\phi_{s\mu}$ and yaw stability extreme state: γ_{max}, β_{max}, and roll stability extreme state: $\varnothing_{max}$. The output parameters of MMCCS include steering wheel Angle δ_{ste}, the driving torque of each in-wheel motor ΔT_{dfl}, ΔT_{dfr}, ΔT_{drl}, ΔT_{drr}, and the braking torque of each wheel ΔT_{xfl}, ΔT_{xfr}, ΔT_{xrl}, ΔT_{xrr} and the control force of each quarter suspension ΔF_{xfl}, ΔF_{xfr}, ΔF_{xrl}, ΔF_{xrr}. MMCCS provides parameter input for the control system with the environment perception and road reconstruction components, path planning components and speed planning components in the perception fusion module and decision-planning module and gives full play to the intelligent advantages of WDDV.

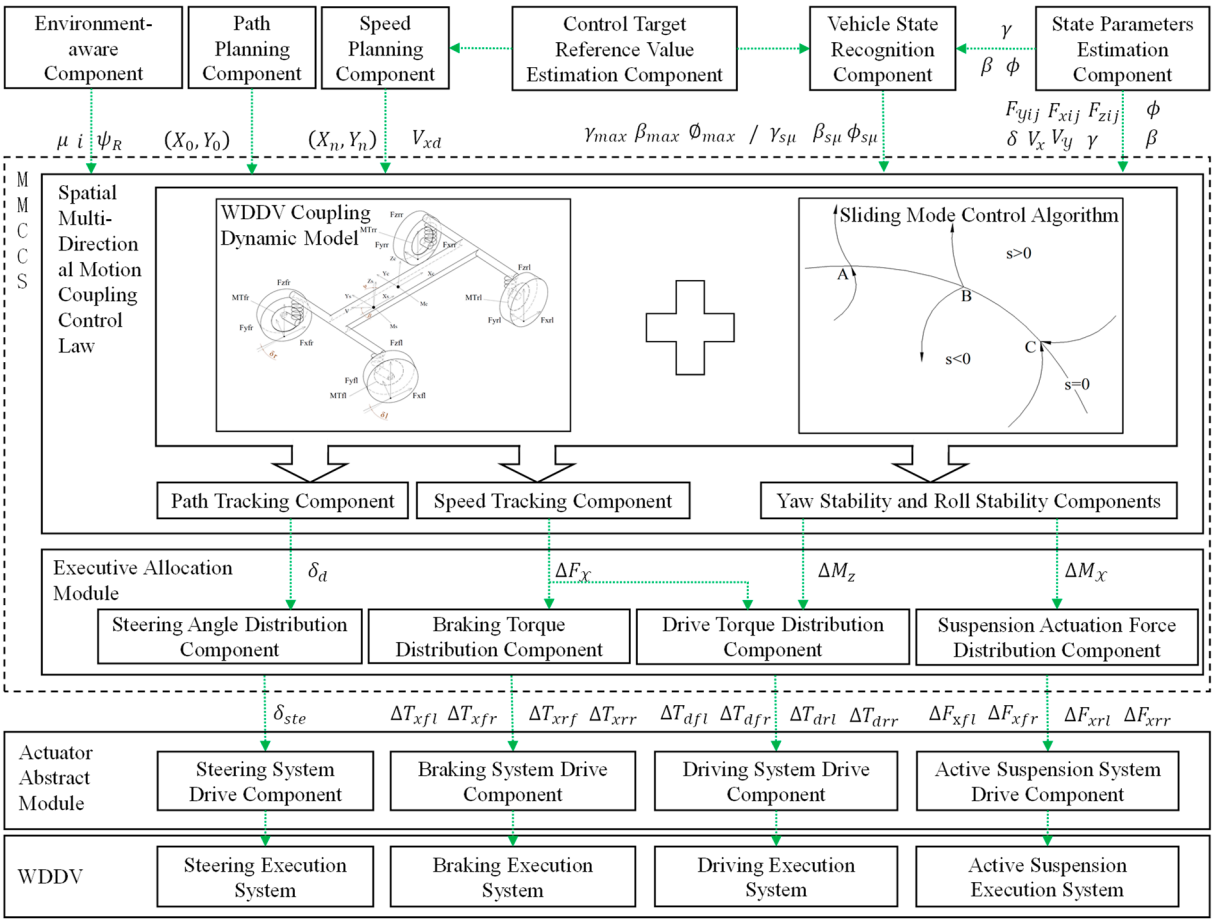

Figure 4. Architecture of MMCCS for a wheel drive driverless vehicle.

2.4.2. Design of Coupled Control Law

The multi-directional motion coupling control law of WDDV encompasses the path tracking law, vehicle speed tracking law, yaw stability control law, and roll stability control law. By incorporating the existing research findings of the author, along with Equations (6)–(9) and the sliding mode control algorithm, the design of the path tracking law, speed tracking law, and yaw stability control law can be achieved [28], which will not be elaborated upon. In this paper, the same approach is adopted to formulate the roll stability control law, considering the wheel drive counter force. The design of the sliding mode for roll stability control is as follows:

$$s_A = \dot{e_A} + c_A e_A \tag{27}$$

where c_A is an adjustable parameter, and $c_A > 0$; e_A is the roll angle tracking error, which is calculated by the current roll angle $\varnothing$ and the target body roll angle $\varnothing_{d\mu}$. According to the cooperative principle of improving the handling of WDDV under conventional conditions and ensuring stability under extreme conditions, the reference value of the roll angle control target is composed of $\varnothing_{s\mu}$ and $\varnothing_{max}$. The specific expression for $\varnothing_{d\mu}$ is as follows:

$$e_A = \varnothing - \varnothing_{d\mu} \tag{28}$$

$$\varnothing_{d\mu} = \begin{cases} \varnothing_{s\mu}, & |\varnothing_{s\mu}| < |\varnothing_{max}| \\ \varnothing_{max}, & |\varnothing_{s\mu}| \geq |\varnothing_{max}| \end{cases} \tag{29}$$

Using the saturation function $sat(s_A)$ replaces the sign function $sgn(s_A)$ [50], and a new exponential-reaching law is obtained as follows:

$$\dot{s_A} = -\varepsilon_A \cdot sat(s_A) - k_A s_A \tag{30}$$

where ε_A is an adjustable parameter; k_A is an adjustable parameter.

Combined with Equations (9), (27), (28) and (30), the sliding mode control law for calculating the roll control torque $\Delta M_{\mathcal{X}}$ is as follows:

$$\Delta M_{\mathcal{X}} = -I_x \left[\varepsilon_A \, sat(s_A) - \ddot{\varnothing}_{d\mu} + c_A\left(\dot{\varnothing} - \ddot{\varnothing}_{d\mu}\right) + k_A\left(\dot{\varnothing} - \ddot{\varnothing}_{d\mu}\right) + c_A\left(\varnothing - \varnothing_{d\mu}\right)\right] - [D_{\varnothing}\dot{\varnothing} + I_{XZ}\dot{\gamma} + \varnothing(C_{\varnothing} - gh_u m_u) + a_y h_u m_u + \Delta_{df}\left(F_{y_{fr}} + F_{y_{fl}}\right)cos\delta + \Delta_{dr}(F_{y_{rr}} + F_{y_{rl}}) + M_{zs}] \tag{31}$$

Using Lyapunov's second stability criterion, the stability analysis of the control system composed of the designed roll stability control law is carried out. The Lyapunov function is defined as $V_A = {s_A}^2/2$. Then $\dot{V_A} \leq -\varepsilon_A|s_A| - k_A{s_A}^2$ can be obtained from Equation (30). $\varepsilon_A > 0$, $k_A > 0$, $|s_A| \geq 0$, ${s_A}^2 \geq 0$, so $\dot{V_A} \leq 0$. Therefore, the roll stability control system is asymptotically stable.

During roll control, the objective is to minimize the discrepancy between the roll angles induced by the roll control force in both the front and rear suspensions, aiming to prevent the emergence of supplementary torsional moments on the vehicle's front and rear bodies. The computation equation for the supplementary suspension-induced driving force is expressed as follows:

$$\Delta F_{xfl} = \frac{\Delta M_{\mathcal{X}}\left(F_{zfl} + F_{zfr}\right)}{F_z d_f} \tag{32}$$

$$\Delta F_{xfr} = -\Delta F_{xfl} \tag{33}$$

$$\Delta F_{xrl} = \frac{\Delta M_{\mathcal{X}}(F_{zrl} + F_{zrr})}{F_z d_r} \tag{34}$$

$$\Delta F_{xrr} = -\Delta F_{xrl} \tag{35}$$

where ΔF_{xfl} is the control force of the left front suspension; ΔF_{xfr} is the control force of the right front suspension; ΔF_{xrl} is the control force of the left rear suspension; and ΔF_{xrr} is the control force of the right rear suspension.

3. Experiments and Results Analysis

3.1. Simulation Research

To validate the efficacy of the proposed multi-directional motion coupling control methodology, a simulation analysis is conducted employing a representative WDDV model. The example WDDC model's principal parameters are enumerated in Table 1, at which point the vehicle dynamics model is established in CarSim, taking into consideration the data provided therein. Through thorough validation against prototype vehicle experimental data and comparative analysis with analogous models, the CarSim model demonstrates a commendable level of simulation accuracy. The MMCCS model is implemented in Matlab 2021a/Simulink, while the performance assessment entails a comparative analysis between the MMCCS and a decoupling control system (DCS). The control law for the DCS, detailed in the author's prior research endeavors [28], adheres to conventional control methodologies.

Table 1. Main WDDV parameters.

Symbol	Description	Value (Unit)
m	Vehicle mass	1798 (kg)
m_f	springing mass of the front suspension	150 (kg)
m_r	springing mass of the rear suspension	150 (kg)
a	Distance from center of gravity to front axle	1.050 (m)
b	Distance from center of gravity to rear axle	1.620 (m)
d_f	Front wheel track	1.565 (m)
d_r	Rear wheel track	1.565 (m)
h_c	Height of vehicle center of gravity	0.650 (m)
I_x	Roll moment of inertia of vehicle	700.7 (kg·m^2)

Table 1. *Cont.*

Symbol	Description	Value (Unit)
I_y	Pitch moment of inertia of vehicle	2059.2 (kg·m^2)
I_z	Yaw moment of inertia of vehicle	2059.2 (kg·m^2)
J_w	Rotational inertia of the wheel	0.85 (kg·m^2)
R	Wheel rolling radius	0.347 (m)

3.1.1. Setting Conditions

To fulfill the requirements for evaluating the control effectiveness and advantages of the MMCCS, the simulation scenario design encompasses a comprehensive range of driving conditions for the WDDV, including both conventional and extreme scenarios. The following specifications are defined for the solution configuration, encompassing road conditions and driving regulations within the simulation framework:

(1) The simulation adopts a time step of 0.01 s.

(2) The initial velocity of the WDDV is initialized to 0 km/h.

(3) The selection of the target path aims to encapsulate the complex operational conditions encountered during vehicle maneuvering, thereby facilitating an assessment of the vehicle's handling and stability control efficacy across normal and extreme scenarios. In adherence to industry-standard procedures for evaluating vehicle handling and stability, the target path is designed as a composite trajectory, combining a double lane change condition with a serpentine condition, as visually depicted in Figure 5.

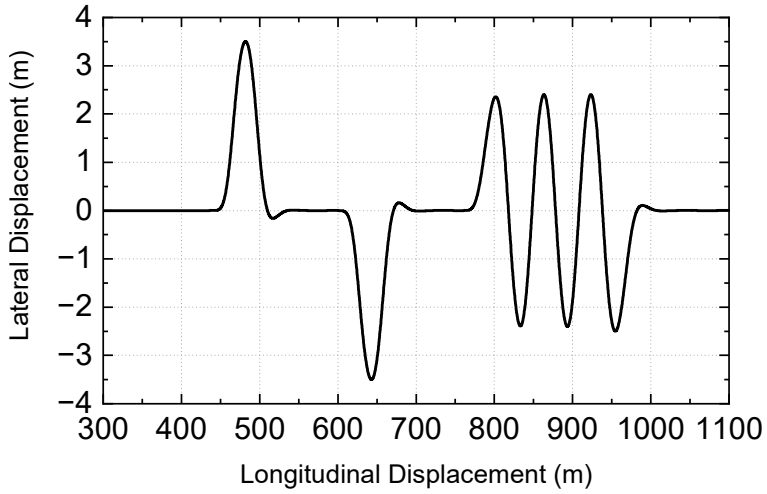

Figure 5. The target path.

(4) To conduct a comprehensive evaluation of the control system, a diverse set of test roads was designed. Under each road condition, including extreme and conventional speeds, corresponding test analyses were performed. Due to space limitations, this article focuses on the analysis of dry road and ice-snow road scenarios as exemplars. The adhesion coefficient for the dry road is 0.8, while for the ice and snow road, it is 0.15. The extreme speed planning methodology for each respective road condition is as follows: the principle is to ensure that the vehicle does not exceed the extreme speed and that the vehicle's speed is reduced to a safe level before entering the corner. The conventional speed is significantly lower than the extreme speed. Under dry road conditions, the corresponding speeds relating to the target path are displayed in Figure 6a. In this figure, V_{x_maxf} represents the maximum target speed limit, V_{xdf} denotes the extreme speed planned by the WDDV speed planning component, adhering to the principle of not surpassing V_{x_maxf} and reducing the speed to a safe level before turning and V_{xdl} represents the significantly lower conventional speed.

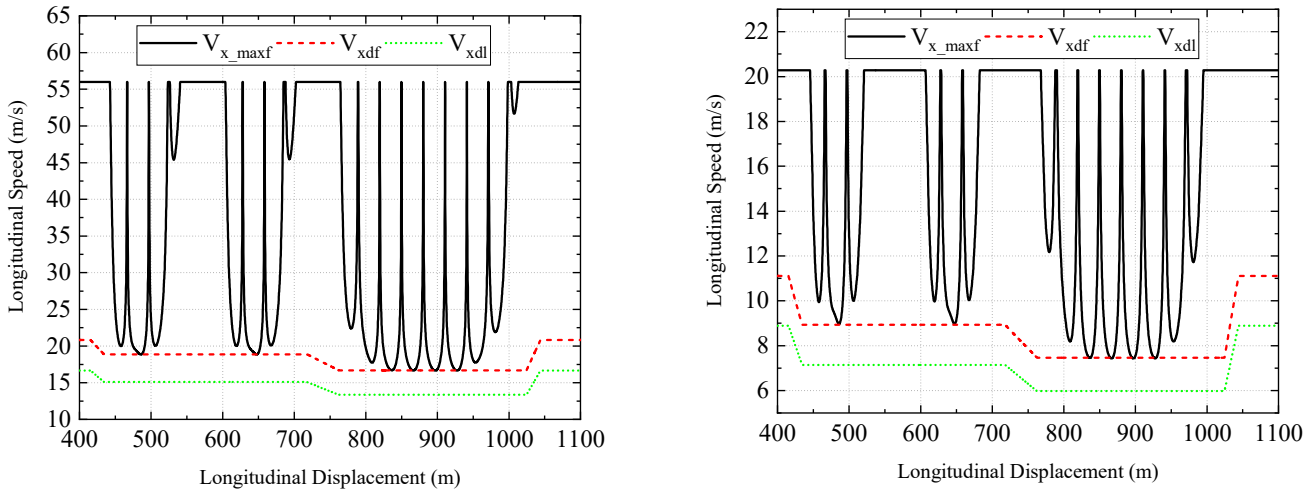

Figure 6. (**a**) The various speeds correspond to the dry road. (**b**) The relevant speed corresponds to the ice-snow road.

WDDV is driven under the target path illustrated in Figure 5 at both extreme speed V_{xdf} and conventional speed V_{xdl}. The lateral acceleration response is presented in Figure 7a, where a_{yf} represents the lateral acceleration response at extreme speed V_{xdf}, and a_{yl} represents the lateral acceleration response at the normal speed V_{xdl}. As observed in Figure 7a, the maximum value of a_{yf} reaches 7.31 m/s^2, which closely approximates the lateral acceleration limit of 7.84 m/s^2 that the vehicle can achieve on the dry road with an adhesion coefficient of 0.8. This finding substantiates the reasonableness of the chosen extreme speed V_{xdf}, which enables WDDV to operate under extreme conditions. Furthermore, the maximum value of a_{yl} amounts to 4.56 m/s^2, significantly lower than 7.84 m/s^2. This demonstrates that the set conventional speed V_{xdl} is rational and enables WDDV to operate under conventional conditions. For the ice-snow road condition, the corresponding speeds associated with the target path are depicted in Figure 6b.

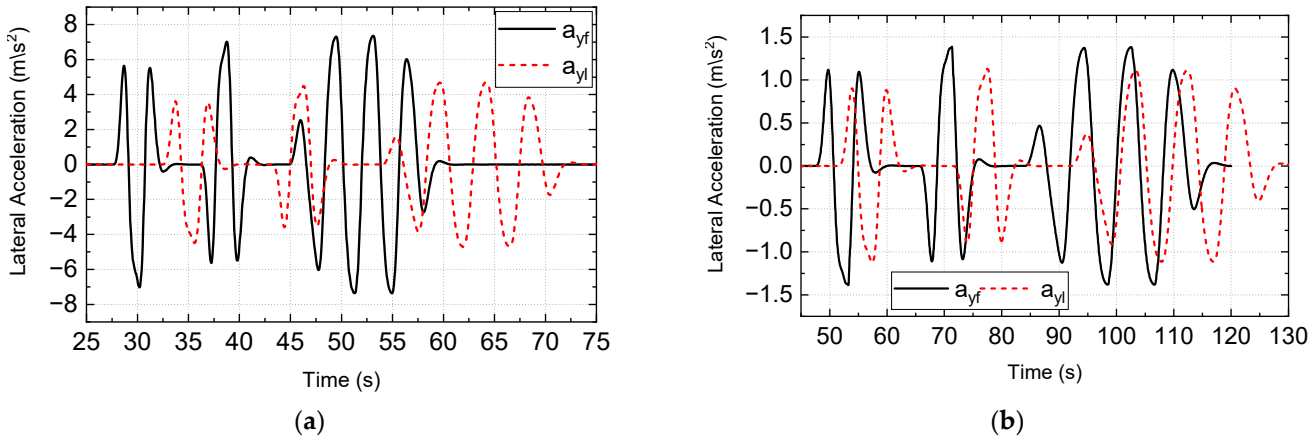

Figure 7. (**a**) The lateral acceleration corresponds to various speeds under dry road conditions. (**b**) The lateral acceleration corresponds to various speeds under ice-snow road conditions.

Analogous to the ice-snow road conditions, the lateral acceleration responses corresponding to the respective speeds are presented in Figure 7b. Through the same analytical process applied to each vehicle's speed and its corresponding lateral acceleration under dry road conditions, it can be concluded that the planned extreme speed and set conventional

speed are reasonable and consistent. For brevity, further repetition of the analysis process will be omitted.

3.1.2. Verification of Validity

The control system comprises MMCCS and DCS, with the vehicle dynamics model established in CarSim serving as the controlled object. The simulation test was conducted based on the aforementioned settings. In the subsequent simulation results, the No.1 curve represents the effect results of MMCCS, while the No.2 curve represents the effect results of DCS.

Under conventional conditions, WDDV operates at the conventional speed V_{xdl} on both the dry road and the ice-snow road, following the target path depicted in Figures 5 and 6a,b, respectively. Considering the emphasis on handling under conventional conditions, the lateral error and longitudinal speed error outcomes are presented in Figures 8 and 9. The figures indicate that the absolute values of lateral error and longitudinal speed error for both control systems on the dry road do not exceed 0.03 m and 0.007 m/s, respectively. On the ice-snow road, the absolute value of lateral error remains below 0.013 m, while the absolute value of longitudinal speed error does not exceed 0.006 m/s. To facilitate a quantitative evaluation of the control effectiveness, the simulation results were organized, and a summary of the simulation outcomes under conventional conditions is presented in Table 2.

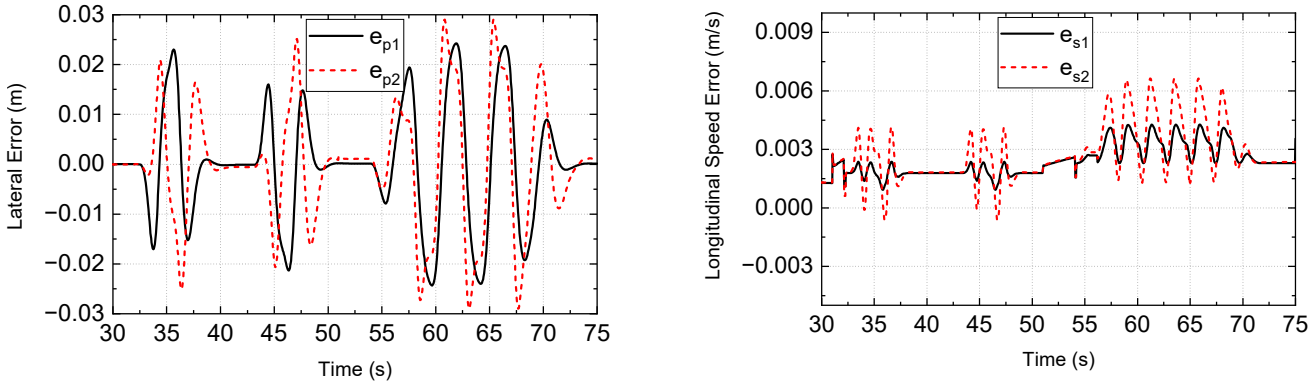

(**a**) (**b**)

Figure 8. Comparison of the path tracking error. (**a**) The speed tracking error. (**b**) Two algorithms on the dry road.

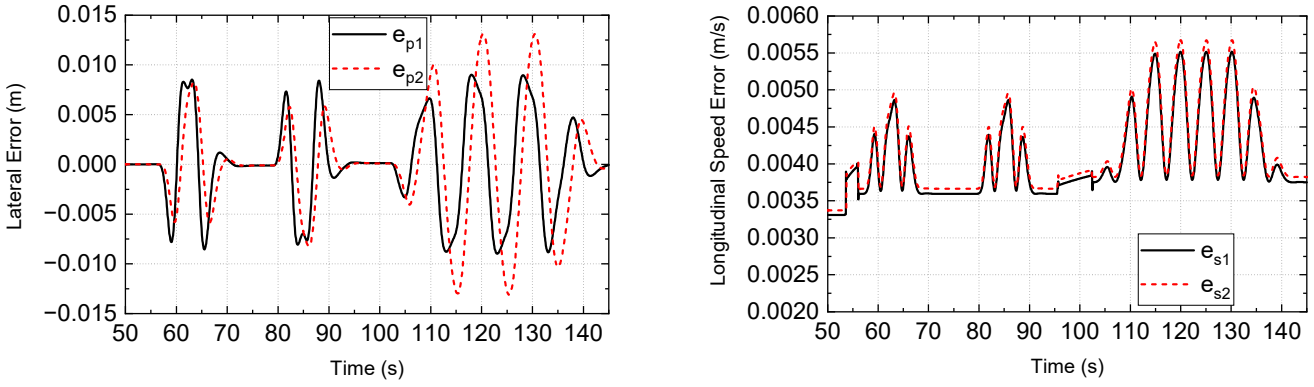

(**a**) (**b**)

Figure 9. Comparison of the path tracking error. (**a**) The speed tracking error. (**b**) Two algorithms on the ice-snow road.

Table 2. Summary of simulation results of double-shift line driving and serpentine driving under conventional conditions.

Control System		DCS		MMCCS		Improvement Rate
μ	Parameters (Units)	Min	Max	Min	Max	
0.8	e_P (m)	−0.029	0.029	−0.024	0.024	17%
	e_s (m/s)	−0.001	0.007	−0.001	0.004	43%
0.15	e_P (m)	−0.013	0.013	−0.009	0.009	31%
	e_s (m/s)	0.004	0.006	0.003	0.005	17%

The improvement rate in the table is calculated relative to the DCS control results and is calculated according to the larger absolute value of the upper and lower boundaries of the corresponding parameter variation range. For example, e_s for the road adhesion coefficient is 0.8, from the data in the table: abs (−0.001) < abs (0.007), and abs (−0.001) < abs (0.004), so the optimized ratio is [abs (0.007) − abs (0.004)]/abs (0.007) ≈ 43%. The improvement rate is positive, indicating performance improvement.

Figures 8 and 9 demonstrate that the MMCCS and DCS effectively achieve path-tracking control and vehicle speed-tracking control for WDDV in conventional scenarios. Consequently, both MMCCS and DCS exhibit favorable handling control performance on WDDV. Furthermore, MMCCS demonstrates superior performance in minimizing lateral error and longitudinal speed error when compared to DCS, particularly in dry and ice-snow road conditions under conventional circumstances. Table 2 illustrates that the reduction in peak lateral error ranges from 17% to 31%, while the reduction in peak longitudinal speed error ranges from 17% to 43%. It is proved that the control expectation state estimation method proposed in this paper can estimate the expected dynamic response of the virtual driver more accurately than the traditional method. The control strategy is used to control the vehicle to track the estimated control desired state in this paper, which is more conducive to improving the path tracking accuracy and vehicle speed tracking accuracy. Thus, MMCCS proves to be more conducive to enhancing the handling of WDDV than DCS in conventional conditions.

The evaluation of the control effect of WDDV under extreme conditions necessitates careful consideration of stability assessment parameters while ensuring that the handling evaluation parameters remain within an acceptable range. Utilizing the extreme speed V_{dx_f} depicted in Figure 6a for both dry and ice-snow road conditions, the response outcomes of lateral error, longitudinal speed error, yaw rate, sideslip angle, and roll angle, resulting from WDDV driving along the target path illustrated in Figure 5, are presented in Figures 10–14.

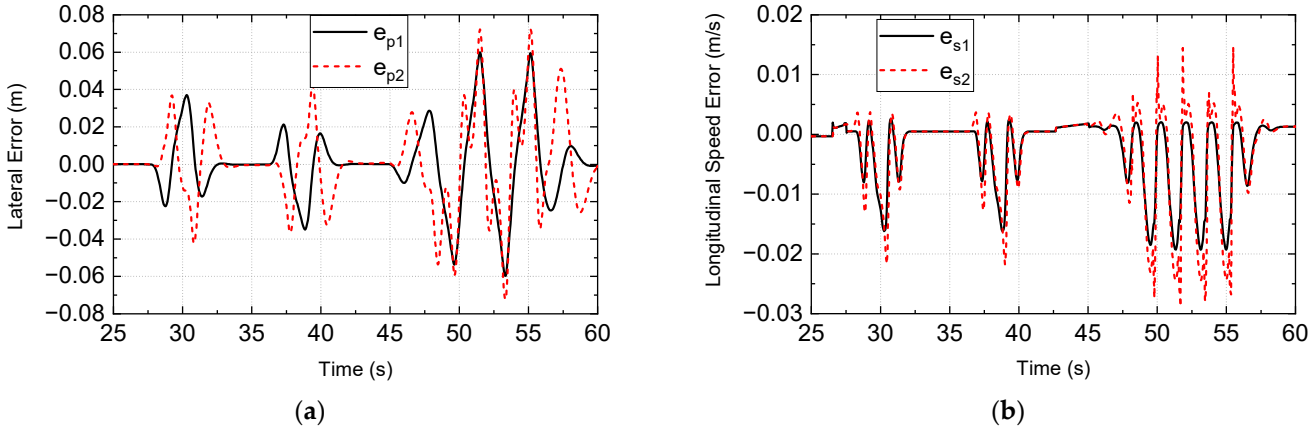

Figure 10. The comparison of the path tracking error. (**a**) The speed tracking error. (**b**) The dry road.

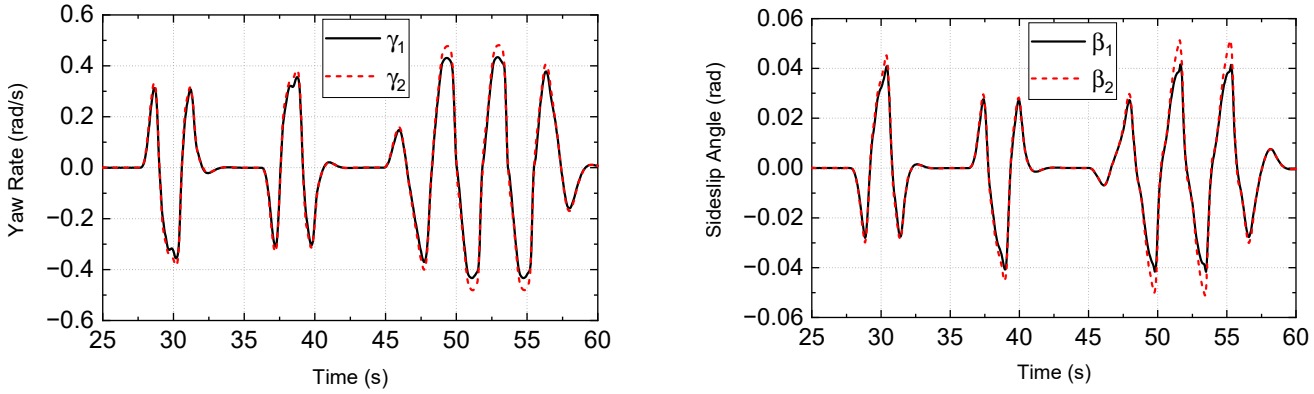

(**a**) (**b**)

Figure 11. The comparison of the yaw rate. (**a**) The sideslip angle (**b**) The dry road.

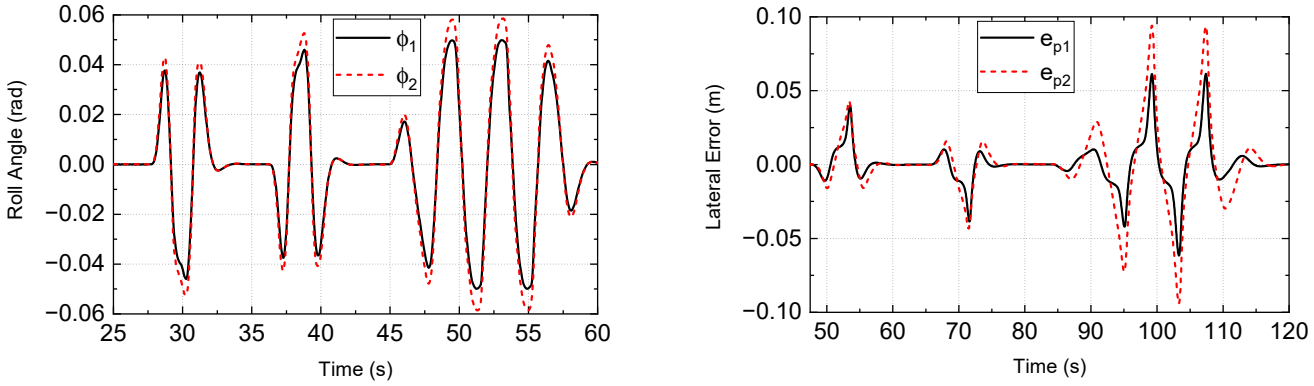

(**a**) (**b**)

Figure 12. The comparison of the roll angle. (**a**) The dry road and the path tracking error. (**b**) The ice-snow road.

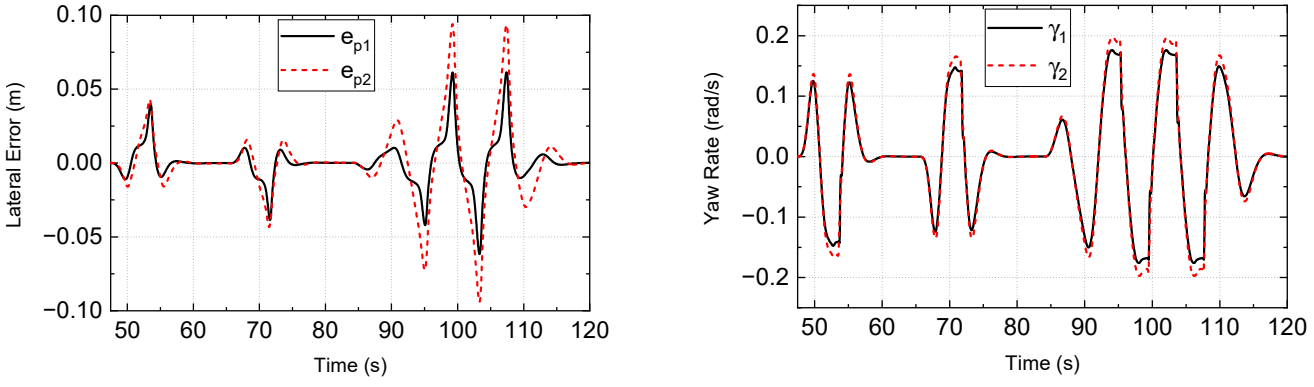

(**a**) (**b**)

Figure 13. The comparison of the speed tracking error. (**a**) The yaw rate. (**b**) The ice-snow road.

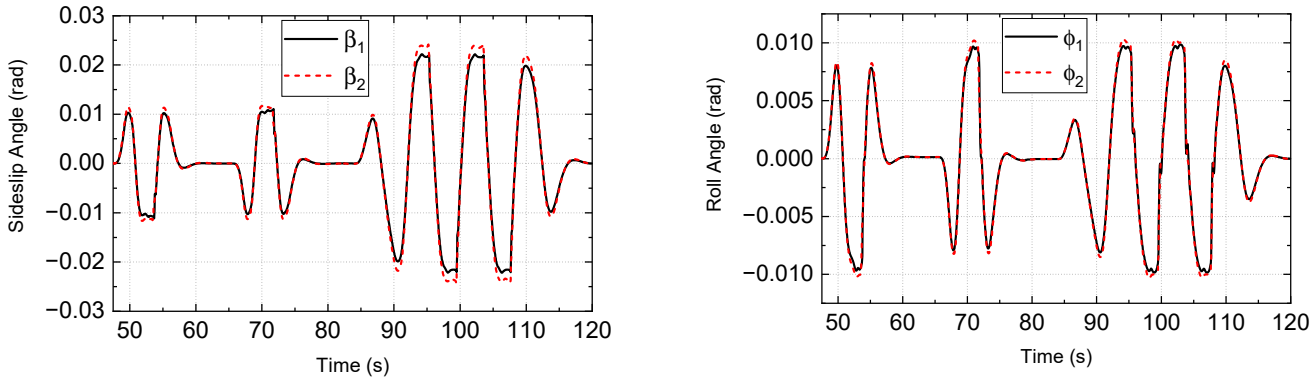

Figure 14. The comparison of the sideslip angle. (**a**) The roll angle. (**b**) The ice-snow road.

Figure 10a,b illustrate that under the extreme conditions corresponding to the dry road, the absolute value of lateral error remains within 0.08 m, while the absolute value of longitudinal speed error remains within 0.03 m/s. Similarly, Figures 12b and 13a demonstrate that under the extreme conditions associated with the ice-snow road, the absolute value of lateral error does not exceed 0.1 m, and the absolute value of longitudinal speed error does not surpass 0.06 m/s. Both control systems effectively ensure that WDDV exhibits the required handling under these extreme conditions.

Figure 11, Figure 12a, Figure 13b, and Figure 14 indicate that MMCCS exhibits a narrower range of control over the yaw rate, sideslip angle, and roll angle of WDDV compared to DCS under both road conditions, thereby enhancing the stability of WDDV. Specifically, under extreme ice-snow road conditions, the stability evaluation parameter range of MMCCS is smaller than that of DCS, whereas this distinction is less pronounced under extreme dry and wet road conditions. These findings suggest that the ability of the handling and stability control system to improve WDDV's stability becomes limited under extremely low adhesion conditions on icy and snowy roads. To quantitatively evaluate the control effect of MMCCS and DCS under extreme conditions, the simulation results of WDDV during double lane changes and serpentine road sections were analyzed, and a summary of the simulation outcomes is presented in Table 3.

Table 3. Summary of simulation results of double-shift line driving and serpentine driving under extreme conditions.

Control System		DCS		MMCCS		Improvement Rate
μ	Parameters (Units)	Min	Max	Min	Max	
0.8	e_P (m)	−0.072	0.072	−0.06	0.06	17%
	e_s (m/s)	−0.029	0.014	−0.019	0.003	34%
	γ (rad/s)	−0.474	0.474	−0.433	0.432	9%
	β (rad)	−0.051	0.051	−0.044	0.042	14%
	ϕ (rad)	−0.058	0.058	−0.05	0.05	14%
0.15	e_P (m)	−0.093	0.093	−0.062	0.061	33%
	e_s (m/s)	0.003	0.006	0.003	0.006	0%
	γ (rad/s)	−0.197	0.197	−0.176	0.175	11%
	β (rad)	−0.024	0.024	−0.022	0.022	8%
	ϕ (rad)	−0.01	0.01	−0.009	0.009	10%

The improvement rate in the table is calculated relative to the DCS control results and is calculated according to the larger absolute value of the upper and lower boundaries of the corresponding parameter variation range. For example, e_s with a road adhesion coefficient of 0.8, from the data in the table: abs (−0.029) > abs (0.014), and abs (−0.019) > abs (0.003), so the optimization ratio is [abs (−0.029) − abs (−0.019)]/abs (−0.029) ≈ 34%. The positive improvement rate indicates improved performance.

Based on the data in Table 3, the following conclusions can be drawn: (1) Under extreme conditions, MMCCS is more effective than DCS in enhancing WDDV's handling. The improvement rate for reducing the peak lateral error ranges from 17% to 33%, while the improvement rate for reducing the peak longitudinal speed error ranges from 0% to 34%. (2) Under extreme conditions, compared to DCS, MMCCS achieves an improvement rate for reducing the peak yaw rate ranging from 9% to 11% and an improvement rate for reducing the peak sideslip angle ranging from 8% to 14%. This indicates that MMCCS demonstrates superior yaw stability control. Additionally, the improvement rate for reducing the peak roll angle ranges from 10% to 14%, indicating that MMCCS exhibits better roll stability control. It is proved that the stability limit state estimation method proposed in this paper can more accurately estimate the dynamic response of the vehicle to maintain stable driving under extreme conditions than the traditional method. Through the control strategy, the vehicle is controlled to track the stable extreme state estimated in this paper, which is more conducive to reducing yaw rate, sideslip angle and body roll angle. At the same time, the above conclusions also prove that the coupling control method proposed in this paper takes into account the longitudinal motion, lateral motion, yaw motion and roll motion and coupling effect of WDDV, and avoids the control conflict of each direction motion, so it can improve the yaw and roll stability while reducing the lateral path tracking error and longitudinal speed tracking error. These results confirm that MMCCS is more effective in improving the stability of WDDV under extreme conditions. The above conclusions demonstrate that, in comparison to DCS, MMCCS offers more effective control over the dynamic response of WDDV during extreme driving conditions, thereby enhancing both handling and stability.

3.2. Experimental Verification

The assessment of MMCCS's actual control effectiveness primarily relies on real vehicle testing, which entails significant costs, lengthy research and development cycles, and substantial security risks. However, the testbed test partially addresses the limitations of pure digital simulation, offering benefits such as a secure testing process, reduced testing costs, shorter debugging and optimization cycles, and better control over the testing environment. To further validate the suitability of MMCCS for extreme conditions in practical applications, experimental verification was conducted as an extension of the initial pure digital simulation verification process.

3.2.1. Building a Testbed

The testbed for MMCCS comprises two distinct components: the software system and the hardware system.

The software system of the testbed encompasses two key elements: the central computing unit and the virtual WDDV. Following industry practices, the central computing unit's software system consists of the Ubuntu operating system and ROS. The MMCCS C++ code, derived from the automatic conversion of Matlab/Simulink, operates within the ROS framework on the central computing unit of the WDDV. The virtual WDDV terminal model primarily encompasses the controlled object's WDDV model. To better compare with the pure digital simulation results, the model uses the same controlled WDDV model as the pure digital simulation verification, and the model is established in CarSim. Figure 15 depicts the software platform architecture of the testbed.

During the operation of the autonomous vehicle, the control system's computational power and the communication interface's capabilities are subjected to stringent requirements. To meet these demands, an industrial control computer is employed as the central computing platform in the implementation of the driverless vehicle. As a result, the industrial control computer functions as the physical controller in the WDDV's testing. Internally, the industrial control computer's functionality is realized through the automatic compilation of program code using Matlab/Simulink. In the experimental setup, a personal laptop serves as the virtual WDDV simulation platform, with the joint simulation

of Matlab/Simulink and CarSim facilitating the creation of the virtual WDDV. The data communication between the industrial control computer and the laptop is established through the dual-channel Kvaser Memorator Pro CAN analyzer. Figure 16 illustrates the testbed configuration for MMCCS.

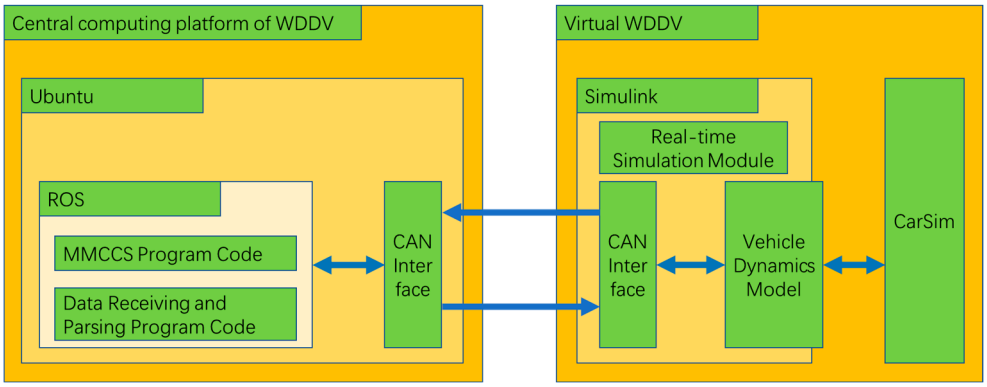

Figure 15. Architecture of the testbed software platform.

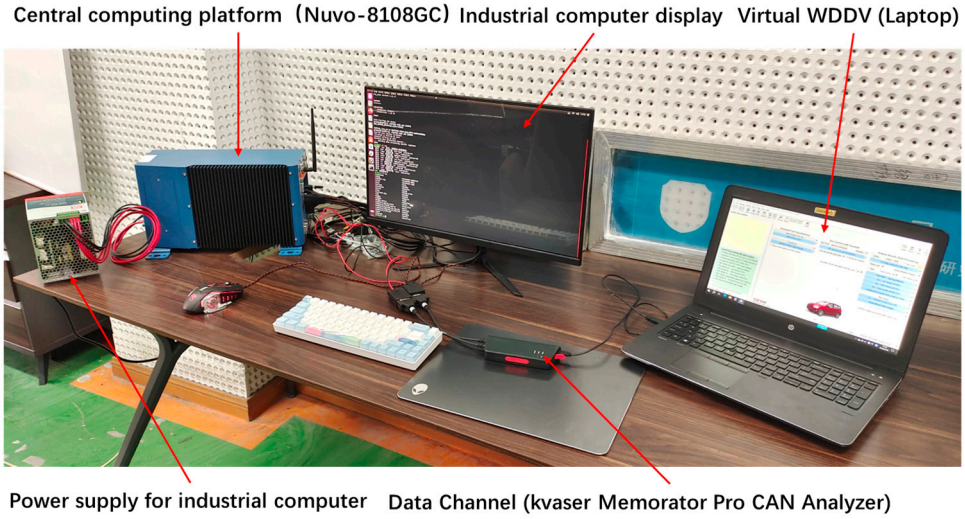

Figure 16. The testbed of MMCCS.

3.2.2. Verifying the Adaptability of Extreme Conditions

The verification of MMCCS's adaptability to extreme conditions in a real controller environment was accomplished by comparing the outcomes of both pure digital simulation tests and testbed tests. The verification process encompassed the same solution settings, comprehensive road conditions, and driving rule designs as described in the aforementioned pure simulation test. In the subsequent analysis, the simulation test results are denoted as X_{sim}, while the testbed test results are represented as X_{hil}.

Figures 17–21 illustrate the response results of lateral error, longitudinal speed error, yaw rate, sideslip angle, and roll angle exhibited by the WDDV while driving under extreme conditions on both dry and ice-snow roads. Figures 17, 18 and 19a demonstrate the comparison between the testbed test results and the pure digital simulation test results under extreme conditions encountered on dry roads. The following observations can be made: (1) The response trends of each parameter were consistent between the two test methods. (2) Both lateral error and longitudinal speed error exhibited significant increases. The absolute value of lateral error ranged from 0.15 m, while the absolute value of longitudinal speed error ranged from 0.025 m/s. Despite these increases, the magnitudes of both errors remained within acceptable limits. (3) The yaw rate and sideslip angle displayed slight increases, exhibiting a satisfactory correspondence. (4) Notably, the roll

angle demonstrated a significant increase, but its absolute value was effectively controlled within the range of 0.062 rad.

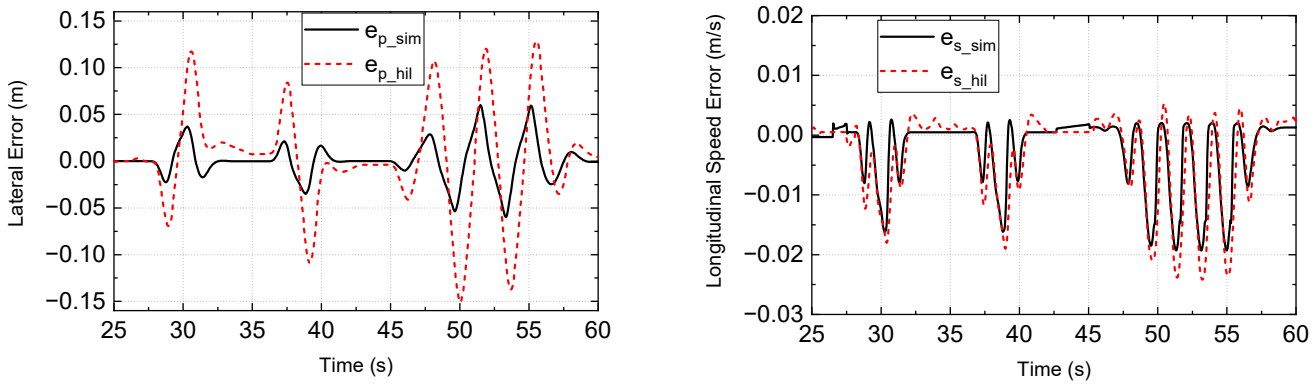

(**a**) (**b**)

Figure 17. The comparison of testbed test results and digital simulation test results. (**a**) The path tracking error. (**b**)The speed tracking error on the dry road.

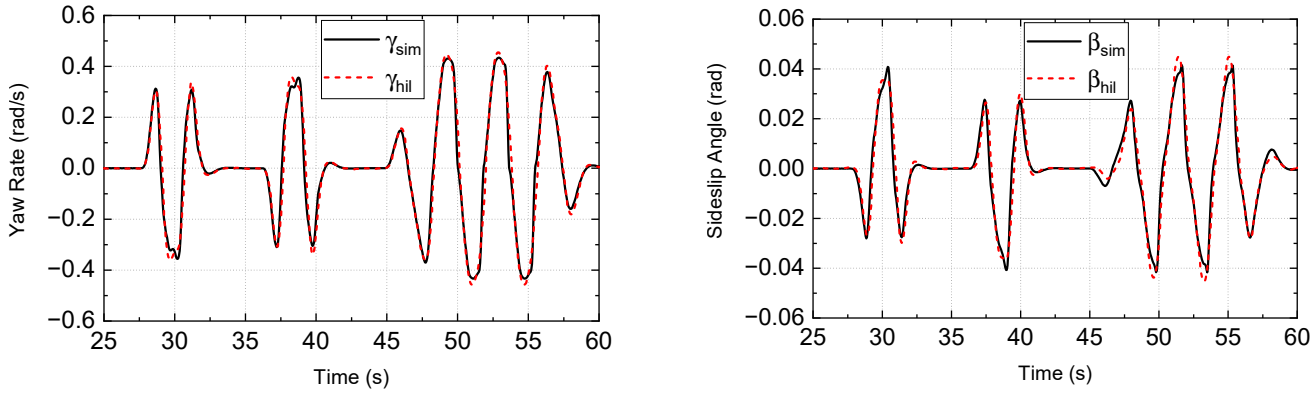

(**a**) (**b**)

Figure 18. The comparison of testbed test results and digital simulation test results. (**a**) The yaw rate. (**b**) The sideslip angle on the dry road.

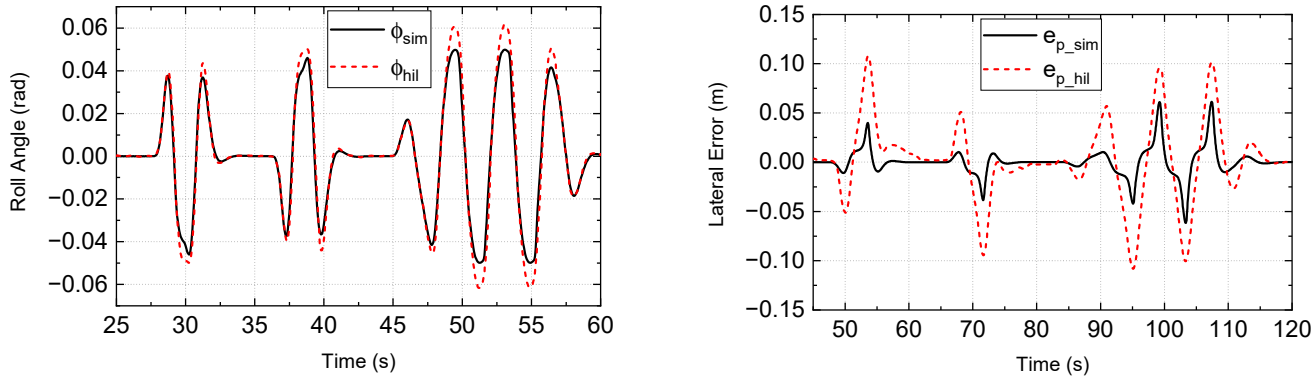

(**a**) (**b**)

Figure 19. The comparison of testbed test results and digital simulation test results. (**a**) shows the roll angle on the dry road. (**b**) The path tracking error on the ice-snow road.

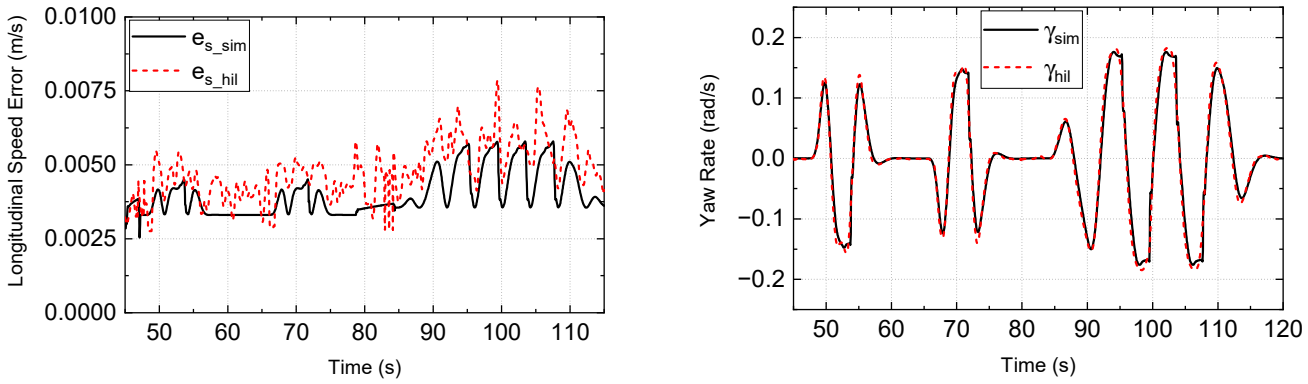

(**a**) (**b**)

Figure 20. The comparison of testbed test results and digital simulation test results. (**a**) The speed tracking error. (**b**) The yaw rate on the ice-snow road.

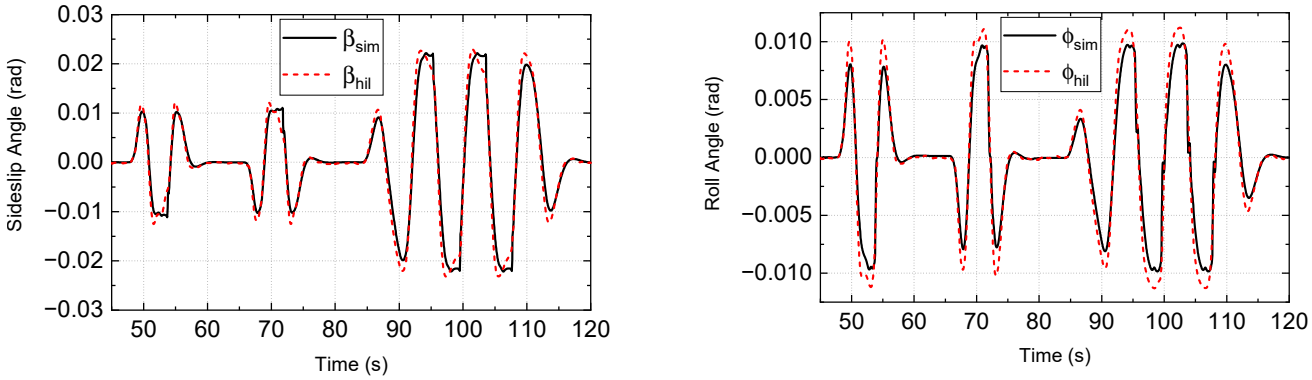

(**a**) (**b**)

Figure 21. The comparison of testbed test results and digital simulation test results. (**a**) The sideslip angle. (**b**) The roll angle on the ice-snow road.

Figures 19b, 20 and 21 present a comparative analysis between the testbed test results and the results obtained from the pure digital simulation test under extreme conditions simulated on ice and snow-covered roads. The following observations can be made: (1) Lateral error response trends were consistent, but the values were quite different. (2) The lateral error and the longitudinal speed error increased significantly. The absolute value of lateral error was in the range of 0.11 m, and the absolute value of longitudinal speed error was in the range of 0.0076 m/s. The values of the two errors are still within the acceptable range. (3) The yaw rate and the sideslip angle increased slightly, and the correspondence is good. (4) Noticeable increase in roll angle: the roll angle exhibited a significant increase, but effective control measures limited its absolute value to within the range of 0.012 rad.

The above phenomena show that in the testbed test process, the control ability of MMCCS decreases, and the path tracking error, vehicle speed tracking error and roll angle increase. At this time, the yaw rate and the sideslip angle should also become larger. However, the turning radius of the vehicle is closely related to the yaw rate and the sideslip angle. Because the path tracking error increases too much, it is difficult to control WDDV to drive strictly according to the target path, the turning radius of the vehicle increases, and the yaw rate and the sideslip angle of the center of mass decrease too much. Finally, the phenomenon of the yaw rate and sideslip angle decreasing is shown. Compared to the pure digital simulation test environment, the handling control ability of MMCCS in the testbed test environment experiences a reduction, yet it still meets the fundamental requirements for handling control. The yaw stability control ability remains unchanged,

while the roll stability control ability is diminished, but the preservation of roll stability is still ensured.

The testbed test results indicate the following: (1) In the real controller environment, the handling and stability control ability of MMCCS under extreme conditions experiences a reduction due to code conversion and hardware real-time performance. However, it effectively enables the handling and stability control of WDDV. (2) Within the real controller environment, MMCCS achieves coupled control of longitudinal motion, lateral motion, yaw motion, and roll motion of WDDV under extreme conditions. It ensures stability while satisfying the requirements of handling control, demonstrating commendable real-time control capabilities.

4. Conclusions

This paper analyzes the technical characteristics of vehicle handling stability in the context of driverless systems. It establishes control targets for the handling stability of Wirelessly Driven Driverless Vehicles (WDDV). An 8-DOF coupled dynamic model of WDDV is developed based on its configuration characteristics and control requirements. The study investigates the mechanism of handling and stability, deriving the control expectation state and stable extreme state estimation model for WDDV. Furthermore, the paper designs a Multi-directional Motion Coupling Control System (MMCCS) for WDDV based on the 8-DOF coupled dynamics model, which is verified through digital simulation and testbed verification. In the future work, the contents that need to be improved are as follows: (1) Under extreme conditions, it is difficult to accurately describe the real response through the vehicle model. To verify the application feasibility of the proposed method, real vehicle verification under extreme conditions is needed. (2) The test method of the handling and stability evaluation index and the determination method of index limit for the driverless vehicle need to be further studied. (3) Under the background of electrification and intelligence, the controllable degree of freedom of WDDV is greatly increased. With the complexity of the model, the real-time challenge of the control system will also be brought. How to comprehensively consider the driving conditions and carry out the "degradation" and "evolution" of the model in real-time remains to be further studied.

Author Contributions: Conceptualization, Y.L. and K.W.; formal analysis, L.D.; investigation, Y.L.; methodology, K.W. and Z.W.; resources, H.W.; supervision, Z.W. and K.W.; validation, Y.L. and K.W.; visualization, H.W. and L.D.; writing—original draft, Y.L. and K.W.; writing—review and editing, Y.L. and K.W. All authors have read and agreed to the published version of the manuscript.

Funding: This work was supported by the Talent Project of Chengdu Technological University under Grant 2023RC054, and the Science Laboratory Open Fund Project of Chengdu Technological University under Grant 2023LOF020.

Data Availability Statement: Data are available from authors upon reasonable request.

Conflicts of Interest: The authors declare no conflicts of interest.

Nomenclature

a	Distance from center of gravity to front axle.
a_x	Longitudinal acceleration.
a_y	Lateral acceleration.
a_{ymax}	Maximum lateral acceleration that the vehicle can achieve in stable driving.
A	Windward area of the vehicle.
A_t, B_t, C_t, D_t, E_t, F_t, G_t	Weight coefficients of the handling and stability evaluation paradigm of traditional vehicles.
A_c,B_c, C_c, D_c, E_c, F_c, G_c, H_c	Weight coefficients of the handling and stability evaluation paradigm of the wheel drive driverless vehicle.
b	Distance from center of gravity to rear axle.
$C_\varnothing$	Roll stiffness of the vehicle.
c_A	Adjustable parameter.

C_D	Air resistance coefficient.
$C_{\mathcal{Y}f}$	Equivalent slip angle stiffness of the front axle tires.
$C_{\mathcal{Y}r}$	Equivalent slip angle stiffness of the rear axle tires.
$D_{\emptyset}$	Roll-damping coefficient of the vehicle.
DCS	Decoupling control system.
d_f	Front wheel track.
d_r	Rear wheel track.
e_A	Roll angle tracking error.
e_P	Lateral error.
e_s	Longitudinal speed error.
$f\left(\sigma_f\right)$	Coefficient equation in the Dugoff tire model.
f	Tire rolling resistance coefficient.
$f_{CS}(e_s)$	Evaluation function of vehicle speed tracking test.
$f_H(\gamma)$	Evaluation function of the steering returnability test.
$f_J(\gamma, \beta)$	Evaluation function of the steering wheel angle step input test.
$f_{LJ}(e_P)$	Evaluation function of path tracking test.
$f_M(\gamma)$	Evaluation function of the steering wheel angle pulse test.
$f_Q(F_Q)$	Evaluation function of the steering portability test.
F_Q	Steering force of the steering wheel.
$f_S(\gamma, \delta_s)$	Evaluation function of the serpentine driving test.
$f_{Sc}(\gamma)$	Evaluation function of the serpentine driving test for driverless patterns.
$f_W(\emptyset, \gamma)$	Evaluation function of the steady-state rotation test.
$\Delta F_{\mathcal{X}}$	Longitudinal control force.
ΔF_{xfr}	Control force of the right front suspension.
ΔF_{xfl}	Control force of the left front suspension.
$F_{\mathcal{X}ij}$	Tire's longitudinal force.
ΔF_{xrl}	Control force of the left rear suspension.
ΔF_{xrr}	Control force of the right rear suspension.
$F_{\mathcal{Y}ij}$	Tire lateral force.
$f_Z\left(\gamma, T_Q\right)$	Evaluation function of the test in the central area of the steering wheel.
$f_{Zc}(\gamma)$	Evaluation function of the test for the steering wheel center area of the driverless pattern.
F_{zfx}	Vertical force of the front wheel unilateral tire.
F_{zrx}	Vertical force of the rear wheel unilateral tire of the vehicle.
g	Acceleration of gravity.
h_c	Height of vehicle center of gravity.
H_{sfl}	Suspension height of the first quarter of the left.
H_{sfr}	Suspension height of the right front quarter.
H_{srl}	Suspension height of the left rear quarter.
H_{srr}	Suspension height of the right rear quarter.
h_{u}	Distance from the center of mass of the sprung mass to the roll axis.
i	Longitudinal slope of the road.
I_x	Roll moment of inertia of vehicle.
I_{xz}	Inertial product of the whole vehicle in the XZ plane of the vehicle coordinate system.
I_y	Pitch moment of inertia of vehicle.
I_z	Yaw moment of inertia of vehicle.
J_w	Rotational inertia of the wheel.
K	Stability factor.
K_μ	Stability factor derived from the estimation of the expected state of the handling of WDDV.
k_A	Adjustable parameter.
L	Wheelbase.
⇳	Vehicle mass.
m_f	Springing mass of the front suspension.
m_r	Springing mass of the rear suspension.
$\mathrm{m_u}$	Sprung mass of the vehicle.
MMCCS	Multi-directional Motion Coupling Control System.
$\Delta M_{\mathcal{X}}$	Roll control torque.
ΔM_z	Yaw control torque.
M_{zs}	Roll moment generated by wheel drive counter force acting on the body.
N_H	Comprehensive score of the steering returnability test.
N_J	Comprehensive score of the steering wheel angle step input test.
N_M	Comprehensive score of the steering wheel angle pulse test.

N_S	Comprehensive score of the serpentine driving test.
N_W	Comprehensive score of the steady-state rotation test.
N_Q	Comprehensive score of the steering portability test.
N_{ZX}	Comprehensive score of the handling and stability test in the central area of the steering wheel.
P_d	Target path.
R	Wheel rolling radius.
T_{bij}	Wheel braking torque.
ΔT_{dfl}	Driving torque of the front left in-wheel motor.
ΔT_{dfr}	Driving torque of the front right in-wheel motor.
T_{dij}	Wheel driving torque.
ΔT_{drl}	Driving torque of the rear left in-wheel motor.
ΔT_{drr}	Driving torque of the rear right in-wheel motor.
T_Q	Steering wheel torque.
ΔT_{sf}	Torque difference on the left and right sides of the front axle.
ΔT_{sr}	Torque difference between the left and right side of the rear axle.
ΔT_{xfl}	Braking torque of the front left wheel.
ΔT_{xfr}	Braking torque of the front right wheel.
ΔT_{xrl}	Braking torque of the rear left wheel.
ΔT_{xrr}	Braking torque of the rear right wheel.
V	Vehicle speed.
$V_{\mathcal{X}}$	Longitudinal speed.
V_{xd}	Target vehicle's speed.
$V_{\mathcal{Y}}$	Lateral speed.
WDDV	Wheel Drive Driverless Vehicle.
X_{hil}	Testbed test results X denotes lateral error, longitudinal speed error, yaw rate, sideslip angle, and roll angle.
(X_n, Y_n)	Target path point set.
X_{sim}	Simulation test results X denotes lateral error, longitudinal speed error, yaw rate, sideslip angle, and roll angle.
y_c	Comprehensive evaluation result of the handling and stability.
y_t	Comprehensive evaluation result of passenger vehicle handling and stability.
α_{ro}	Lateral slope of the road.
β_{max}	Limit value of the target sideslip angle.
β	Sideslip angle.
$\beta_{s\mu}$	Sideslip angle expected by the virtual driver.
$\beta_{d'}$	Target sideslip angle.
γ_{max}	Limit value of the target yaw rate.
γ_d	Target yaw rate.
γ	Yaw rate.
$\gamma_{s\mu}$	Yaw rate expected by the virtual driver.
δ	Average angle of the front wheel.
δ_d	Average rotation angle of the expected front wheel to achieve the target path tracking calculation.
Δ_{df}	Lateral offset of the front tire caused by unit roll angle.
Δ_{dr}	Lateral offset of the rear tire caused by unit roll angle.
δ_s	Steering wheel angle.
δ_{ste}	Steering wheel angle.
ε_A	Adjustable parameter.
μ	Road adhesion coefficient.
$\tau_{\varnothing}$	Maximum roll angle safety factor of the vehicle.
τ_γ	Safety factor.
$\phi_{s\mu}$	Expected roll angle of the virtual driver.
ϕ	Roll angle.
$\varnothing_d$	Target body roll angle.
ψ_R	Yaw angle.

References

1. Mosin, M.; Popov, N.; Anibroev, V.; Vilberger, M.; Domakhin, E. Engine power distribution system for four-wheel drive autonomous electric vehicle. *Energy Rep.* **2023**, *9*, 115–122. [CrossRef]
2. Keqiang, L.I.; Yifan, D.A.I.; Shengbo, L.I.; Mingyuan, B.I.A.N. State-of-the-art and technical trends of intelligent and connected vehicles. *Automot. Saf. Energy Saving* **2017**, *8*, 1–14.
3. Huang, H.; Huang, X.; Ding, W.; Yang, M.; Yu, X.; Pang, J. Vehicle vibro-acoustical comfort optimization using a multi-objective interval analysis method. *Expert Syst.* **2023**, *213*, 119001. [CrossRef]

4. Huang, H.; Lim, T.C.; Wu, J.; Ding, W.; Pang, J. Multitarget prediction and optimization of pure electric vehicle tire/road airborne noise sound quality based on a knowledge-and data-driven method. *Mech. Syst. Signal Process.* **2023**, *197*, 110361. [CrossRef]
5. Huang, H.; Huang, X.; Ding, W.; Yang, M.; Fan, D.; Pang, J. Uncertainty optimization of pure electric vehicle interior tire/road noise comfort based on data-driven. *Mech. Syst. Signal Process.* **2022**, *165*, 108300. [CrossRef]
6. Liang, J.; Lu, Y.; Yin, G.; Fang, Z.; Zhuang, W.; Ren, Y.; Li, Y. A Distributed Integrated Control Architecture of AFS and DYC Based on MAS for Distributed Drive Electric Vehicles. *IEEE Trans. Veh. Technol.* **2021**, *70*, 5565–5577. [CrossRef]
7. Liu, J.; Song, J.; Li, H.; Huang, H. Direct yaw-moment control of vehicles based on phase plane analysis. *Proc. Inst. Mech. Eng. Part D J. Automob. Eng.* **2022**, *236*, 2459–2474. [CrossRef]
8. Fan, L.; Wang, J.; Deng, M.; Peng, Y.; Bao, X.; Wei, H. Torque coordinated control of the through-the-road (TTR) 4-wheel-drive (4WD) hybrid vehicle under extreme road conditions. *Sci. Rep.* **2023**, *13*, 11564. [CrossRef] [PubMed]
9. Zhai, L.; Wang, C.; Hou, Y.; Liu, C. MPC-based integrated control of trajectory tracking and handling stability for intelligent driving vehicle driven by four hub motor. *IEEE Trans. Veh. Technol.* **2022**, *71*, 2668–2680. [CrossRef]
10. Zhang, X.; Liang, H.; Wang, X.; Li, Q. Integrated Direct Yaw Control and Antislip Regulation Mixed Control of Distributed Drive Electric Vehicle Using Cosimulation Methodology. *Math. Probl. Eng.* **2022**, *2022*, 6749649. [CrossRef]
11. Zhang, F.; Xiao, H.; Zhang, Y.; Gong, G. Distributed Drive Electric Bus Handling Stability Control Based on Lyapunov Theory and Sliding Mode Control. *Actuators* **2022**, *11*, 85. [CrossRef]
12. Shen, Y.; Zhao, Y.; Deng, H.; Lin, F.; Shen, H. Coordinated control of stability and economy of distributed drive electric vehicle based on Lyapunov adaptive theory. *Proc. Inst. Mech. Eng. Part D J. Automob. Eng.* **2023**, *238*, 1535–1549. [CrossRef]
13. Guo, N.; Zhang, X.; Zou, Y.; Lenzo, B.; Du, G.; Zhang, T. A supervisory control strategy of distributed drive electric vehicles for coordinating handling, lateral stability, and energy efficiency. *IEEE Trans. Transp. Electrif.* **2021**, *7*, 2488–2504. [CrossRef]
14. Huang, C.; Wu, X.; Wu, C.; Wang, J.; Shu, X. Rule-based torque vectoring distribution strategy combined with slip ratio control to improve the handling stability of distributed drive electric vehicles. *Proc. Inst. Mech. Eng. Part D J. Automob. Eng.* **2024**, 09544070231215926. [CrossRef]
15. Liang, J.; Feng, J.; Lu, Y.; Yin, G.; Zhuang, W.; Mao, X. A Direct Yaw Moment Control Framework Through Robust T-S Fuzzy Approach Considering Vehicle Stability Margin. *IEEE/ASME Trans. Mechatron.* **2024**, *29*, 166–178. [CrossRef]
16. Li, J.; Lu, J.; Lu, H.; Wei, H.; Wu, B.; Jiang, P. A novel conservative dynamics envelope of vehicle lateral stability under different tire characteristics. *Proc. Inst. Mech. Eng. Part D J. Automob. Eng.* **2023**, 09544070231206207. [CrossRef]
17. Jin, Z.L.; Liang, X.H.; Zhao, W.Z. Multi-gains Ratio of Steer-by-wire System and Anti-rollover Control for Vehicle. *J. Mech. Eng.* **2020**, *56*, 172–180.
18. Zhang, L.; Ai, W.; Liu, Z.; Zhang, L.; Teng, X. Stability control of energy saving electric vehicle using dynamic nonlinear system state estimation. *Fractals* **2022**, *30*, 2240096. [CrossRef]
19. Junru, Y. A Modeling and Factor Analysis of Safe Speed on Curve Segments. *J. Transp. Inf. Saf.* **2018**, *36*, 1–8.
20. Liang, Z.; Zhao, J.; Liu, B.; Wang, Y.; Ding, Z. Velocity-based path following control for autonomous vehicles to avoid exceeding road friction limits using sliding mode method. *IEEE Trans. Intell. Transp. Syst.* **2022**, *23*, 1947–1958. [CrossRef]
21. Liu, X.M.; Liu, F.; Guo, J.B. Research on stability of high-speed autonomous vehicles based on linear time-varying model predictive control. *Int. J. Veh. Des.* **2023**, *91*, 360–383. [CrossRef]
22. Yao, X.; Gu, X.; Jiang, P. Coordination control of active front steering and direct yaw moment control based on stability judgment for AVs stability enhancement. *Proc. Inst. Mech. Eng. Part D J. Automob. Eng.* **2022**, *236*, 59–74. [CrossRef]
23. Xiang, C.; Peng, H.; Wang, W.; Li, L.; An, Q.; Cheng, S. Path tracking coordinated control strategy for autonomous four in-wheel-motor independent-drive vehicles with consideration of lateral stability. *Proc. Inst. Mech. Eng. Part D J. Automob. Eng.* **2021**, *235*, 1023–1036. [CrossRef]
24. Chen, L.; Xie, Y.; Cai, Y.; Sun, X.; Teng, C.; Zou, K. Stable Tracking Control of Autonomous Vehicles at Extreme Conditions. *Automob. Eng.* **2020**, *42*, 1016–1026.
25. Zhong, L.F.; Peng, Y.H.; Jiang, M. Stability control of distributed drive electric vehicle based on phase plane. *Automob. Eng.* **2021**, *43*, 721–729.
26. Xuan, N.; Liao, X.Y. Handling and Stability Control of Four-wheel Drive Electric Vehicle under Combined Slip Conditions. *J. Mech. Eng.* **2021**, *57*, 205–220.
27. Park, G.; Choi, S.B. A model predictive control for path tracking of electronic-four-wheel drive vehicles. *IEEE Trans. Veh. Technol.* **2021**, *70*, 11352–11364. [CrossRef]
28. Wang, K.; Yang, M.; Li, Y.; Liu, Z.; Wang, H.; Ding, W. Multidirectional motion coupling based extreme motion control of distributed drive autonomous vehicle. *Sci. Rep.* **2022**, *12*, 13203. [CrossRef] [PubMed]
29. Jia, F.J.; Jing, H.H.; Gu, M.Q. Cooperative control of yaw and roll motion for in-wheel motor vehicle with semi-active suspension. *Proc. Inst. Mech. Eng. Part D J. Automob. Eng.* **2022**, *236*, 3–15. [CrossRef]
30. Hajiloo, R.; Khajepour, A.; Zengin, H.; Kasaiezadeh, A.; Chen, S.K. A coupled force predictive control of vehicle stability using front/rear torque allocation with experimental verification. *Veh. Syst. Dyn.* **2022**, *60*, 2541–2563. [CrossRef]
31. Jan, B.; Tomáš, H. Decoupling of vehicle lateral dynamics using four-wheel steering system. In Proceedings of the 23rd International Conference on Process Control (PC), Strbske Pleso, Slovakia, 9 June 2021.
32. Liu, H.; Liu, C.; Han, L.; Xiang, C. Handling and stability integrated control of AFS and DYC for distributed drive electric vehicles based on risk assessment and prediction. *IEEE Trans. Intell. Transp. Syst.* **2022**, *23*, 23148–23163. [CrossRef]

33. Hang, P.; Xia, X.; Chen, X.B. Handling Stability Advancement With 4WS and DYC Coordinated Control: A Gain-Scheduled Robust Control Approach. *IEEE Trans. Veh. Technol.* **2021**, *70*, 3164–3174. [CrossRef]
34. Lei, Y.; Wen, G.; Geng, X.; Fu, Y.; Li, X.; Hu, J. Comprehensive control of steering and braking via a 4WIS-4WID vehicle. *J. Chin. Soc. Mech. Eng.* **2022**, *43*, 303–313.
35. Xu, T.; Zhao, Y.; Deng, H.; Guo, S.; Li, D.; Lin, F. Integrated optimal control of distributed in-wheel motor drive electric vehicle in consideration of the stability and economy. *Energy* **2023**, *282*, 128990. [CrossRef]
36. Wu, X.; Zhou, B.; Wu, T.; Pan, Q. Research on intervention criterion and stability coordinated control of AFS and DYC. *Int. J. Vehicle Des.* **2022**, *90*, 116–141. [CrossRef]
37. Li, W.; Yu, S.; Tan, L.; Li, Y.; Chen, H.; Yu, J. Integrated control of path tracking and handling stability for autonomous ground vehicles with four-wheel steering. *Proc. Inst. Mech. Eng. Part D J. Automob. Eng.* **2023**, 09544070231204249. [CrossRef]
38. Tang, J.; Li, Q.; Wang, Y.; He, D.; Chen, Y. Tracking Control for Autonomous Four-Wheel Independently Driven Vehicle Based on Deep Reinforcement Learning. In Proceedings of the 6th CAA International Conference on Vehicular Control and Intelligence (CVCI), Nanjing, China, 8 December 2022.
39. Jeong, Y.; Kim, D.H.; Youn, M.H.; Park, S.; Li, X.J.; Lee, T. Model Predictive Control-Based Path Tracking with Four-Wheel Independent Steering, Driving, and Braking Autonomous Vehicles on Low Friction Road. In Proceedings of the 23rd International Conference on Control, Automation, and Systems, Yeosu, Republic of Korea, 20 November 2023.
40. Huang, Y.; Yong, S.Z.; Chen, Y. Stability control of autonomous ground vehicles using control-dependent barrier functions. *IEEE Trans. Intell. Veh.* **2021**, *6*, 699–710. [CrossRef]
41. Chen, J.; Shuai, Z.; Zhang, H.; Zhao, W. Path following control of autonomous four-wheel-independent-drive electric vehicles via second-order sliding mode and nonlinear disturbance observer techniques. *IEEE Trans. Ind. Electron.* **2020**, *68*, 2460–2469. [CrossRef]
42. Jeong, Y.; Yim, S. Path tracking control with four-wheel independent steering, driving and braking systems for autonomous electric vehicles. *IEEE Access* **2022**, *10*, 74733–74746. [CrossRef]
43. *GB/T 6323-2014*; Vehicle Handling and Stability Test Method. China Standards Press: Beijing, China, 2014.
44. *QC/T 480-1999*; Vehicle Handling and Stability Index Limits and Evaluation Methods. China National Machinery Industry Bureau: Beijing, China, 1999.
45. *ISO 3888-2: 2002*; Double-Line International Standard Experiment. International Organization for Standardization: Geneva, Switzerland, 2002.
46. Dugoff, H.P.; Fancher, P.S.; Segel, L. An Analysis of Tire Traction Properties and Their Influence on Vehicle Dynamic Performance. *SAE Trans.* **1970**, *79*, 1219–1243.
47. Zhang, L.P.; LI, L.; Qi, B.N. Rollover prevention control for a four in-wheel motors drive electric vehicle on an uneven road. *Sci. China (Technol. Sci.)* **2018**, *61*, 934–948. [CrossRef]
48. Wang, K.; Ding, W.; Yang, M.; Zhu, Q. Dynamic-boundary-based lateral motion synergistic control of distributed drive autonomous vehicle. *Sci. Rep.* **2021**, *11*, 22644. [CrossRef] [PubMed]
49. Yu, Z.S. Vehicle handling and stability. In *Automotive Theory*, 6th ed.; Machine Press: Beijing, China, 2009.
50. Liu, J.K. Introduction to sliding mode variable structure control. In *Sliding Mode Variable Structure Control MATLAB Simulation: Basic Theory and Design Method*, 3rd ed.; Tsinghua University Press: Beijing, China, 2015.